Alpine thermal and structural evolution of the highest external crystalline massif: the Mont-Blanc.

P.H. Leloup, N. Arnaud, E.R. Sobel and R. Lacassin

P.H. Leloup, Laboratoire des Sciences de la terre, UMR CNRS 5570, Université Claude Bernard, 2 rue Raphaël Dubois, 69622 Villeurbanne Cedex, France. herve.Leloup@univ-lyon1.fr

N. Arnaud, Laboratoire de Dynamique de la Lithosphère (LDL), UMR CNRS 5573, I S T E E M - U S T L, Place Eugène Bataillon, 34095 Montpellier Cedex 5, France.

E. R. Sobel, Institut für Geowissenschaften, Universität Potsdam, Postfach 60 15 53, 14415 Potsdam, Germany

R. Lacassin, Laboratoire de Tectonique, Mécanique de la Lithosphère, UMR CNRS 7578, Institut de Physique du Globe de Paris, 4 place Jussieu, 75252 Paris CEDEX 05, France.

Abstract

The alpine structural evolution of the Mont-Blanc, highest point of the Alps (4810m), and of the surrounding area has been re-examined. The Mont-Blanc and the Aiguilles Rouges external crystalline massifs are windows of Variscan basement within the Penninic and Helvetic nappes. New structural, $^{40}Ar/^{39}Ar$ and fission-track data combined with a compilation of earlier P-T estimates and geochronological data give constraints on the amount and timing of the Mont-Blanc and Aiguilles Rouges massifs exhumation. Alpine exhumation of the Aiguilles Rouges was limited to the thickness of the overlying nappes (~10 km), while rocks now outcropping in the Mont-Blanc have been exhumed from 15 to 20 km depth. Uplift of the two massifs started ~22 Ma ago, probably above an incipient thrust: the Alpine sole thrust. At ~12 Ma, the NE-SW trending Mont-Blanc shear zone (MBsz) initiated. It is a major steep reverse fault with a dextral component, whose existence has been overlooked by most authors, that brings the Mont-Blanc above the Aiguilles Rouges. Total vertical throw on the MBsz is estimated to be between 4 and 8 km. Fission-track data suggest that relative motion between the Aiguilles Rouges and the Mont-Blanc stopped ~4Ma ago. Since that time, uplift of the Mont-Blanc has mostly taken place along the Mont-Blanc back-thrust, a steep north-dipping fault bounding the southern flank of the range. The “European roof” is located where the back-thrust intersects the MBsz. Uplift of the Mont-Blanc and Aiguilles Rouges occurred towards the end of motion on the Helvetic basal décollement (HBD) at the base of the Helvetic nappes, but is coeval with the Jura thin-skinned belt. Northwestward thrusting and uplift of the ECM above the Alpine sole thrust deformed the overlying Helvetic nappes, and formed a back-stop, inducing the formation of the Jura arc. In that part of the external Alps, ~NW-SE shortening with minor dextral NE-SW motions appears to have been continuous from ~22Ma until at least ~4Ma ago but may be still active today. A sequential history of the alpine structural evolution of the units now outcropping NW of the Pennine thrust is proposed.

1 Introduction.

Similar to most other collisional mountain belts, the Alps formed as a crustal-scale orogenic wedge (e.g. Mattauer, 1986), in this case above the southward continental subduction of Eurasia below Apulia (Fig. 1b). The southward plunging slab has been imaged on ECORS and NFP20-west seismic reflection profiles down to a depth of ~40 km below the internal zones (e.g. Nicolas et al., 1990; Pfiffner et al., 1997). Within the orogenic wedge, the thrusts propagated northwest towards the European foreland with a succession of flats and ramps (Fig. 1b). In such a framework, the external crystalline massifs (ECM), which underlie most of the highest summits of the Alps with altitudes over 4000m, have been interpreted as recent culminations above of a crustal thrust ramp (e.g., Ménard and Thouvenot, 1987; Butler, 1985; Lacassin et al., 1990). This paper focuses on the highest of the ECM: the Mont-Blanc massif, the "European roof", which towers at 4810m above all other alpine summits. Surprisingly, the alpine-age structure of the highest alpine peak is still disputed, and this has important bearings on alpine deformation kinematics and mechanics as a whole.

For some, the Mont-Blanc is a coherent, crustal-scale sheet limited by faults or shear-zones, and located in the hanging wall of an alpine thrust (e.g.; Bellière, 1956; Eltchaninoff-Lancelot et al., 1982; Butler, 1985). The sedimentary cover rocks above and in front of the Mont-Blanc massif would be separated from the basement by décollement zones and affected by thin-skinned folds and thrusts. For others, the Mont-Blanc massif corresponds to a crustal-scale recumbent anticline forming the core of the Helvetic nappes (e.g., Ramsay, 1981; Epard, 1986; Escher et al., 1988). This would imply no significant differential slip between basement and cover. Such differing structural interpretations correspond to divergent views about the mechanical behavior of continental crust in orogens. Additionally, some authors ascribe the high elevation of the range to an active normal fault bounding its SE flank (Seward and Mancktelow, 1994; Lemoine et al., 2000) or emphasize the role of Tertiary strike-slip tectonics (Gourlay, 1983; Hubbard and Mancktelow, 1992). Finally, in spite of the topographic evidence for recent and strong uplift, thus probably of exhumation, the importance of Tertiary metamorphism and of ductile deformations in presently outcropping rocks has generally been set aside.

Our goal is thus to better understand how and when the Mont-Blanc massif reached high elevations, and what this tells us about exhumation processes in mountain belts.

2 Overview of Mont-Blanc geology.

The Mont-Blanc and Aiguilles Rouges massifs are two of the Alpine external crystalline massifs (ECM) that form a discontinuous belt along the periphery of the Alps (Fig. 1). The ECM are located in the footwall of the Penninic basal thrust.

The Mont-Blanc massif is mostly composed of a calc-alkaline granite (Fig. 2), locally called "Protogine" that constitutes the famous needles of the "Aiguilles de Chamonix". This granite has been dated by Rb/Sr at 316±19 Ma (Bussy et al., 1989) and by U/Pb on zircons at 304±3 Ma (Bussy and Von Raumer, 1993). The granite and related aplitic veins intrude Variscan metamorphic rocks (Fig. 3b) comprising orthogneisses, paragneisses, carbonate lenses, mafic schists and amphibolites (Von Raumer and Neubauer, 1993). In these rocks, the foliations are generally steep and affected by isoclinal folds. To the NW, the Mont-Blanc massif is separated from the Aiguilles Rouges massif by a strip of Mesozoic sedimentary rocks, commonly called “the Chamonix syncline”, outcropping in the Chamonix glacial valley (Fig. 2a). The Aiguilles Rouges are mostly composed of Variscan metamorphic rocks and granites encompassing synclines containing Visean and Westphalian sedimentary rocks (Fig. 2) (Pairis et al., 1993; Bellière et al., 1987). The NE-SW direction of the ranges is probably partly inherited from Mesozoic normal faults associated with the rifting of the alpine ocean (e.g. Eltchaninoff-Lancelot et al., 1982; Gillcrist et al., 1987). The Triassic unconformity is clearly visible in the Aiguilles Rouges and at the northern and southern tips of the Mont-Blanc massif (Fig. 2a). NW of the Aiguille Rouges the Mesozoic sedimentary series of the Sub-Alpine domain is folded above a thick décollement level located in the Liassic black shales. As it has been tilted northwestward by the rise of the Aiguilles Rouges - Mont-Blanc antiformal culmination, the present day geometry of the décollement resembles that of a listric normal fault (Fig. 2b). Laterally towards the NE, this décollement corresponds to the lower limit of the Helvetic nappe stack (Fig. 2), the roots of which have to be found in the Chamonix valley (Ayrton, 1980; Ramsay, 1981) and/or in the Swiss Val Ferret SE of the Mont-Blanc (Grasmück, 1961). Along the SE flank of the Val Ferret, the Penninic basal thrust is a complex zone of stacked thrusts constituting the basal limit of the Penninic nappes. The roots of the Penninic klippes (Fig. 1 and Fig.2), are found in this zone (e.g. Masson, 1976). Thus, the Mont-Blanc and Aiguille Rouges massifs correspond to a basement window within the Alpine sedimentary nappe stack.

3 Alpine structures within the Mont-Blanc and Aiguilles Rouges massifs.

Each of the three steep flanks that bound the Mont-Blanc massif is associated with an alpine structure: the root of the Helvetic nappes to the east, the Mont-Blanc back-thrust to the south and the Mont-Blanc shear zone to the northwest. The topography of the Aiguilles Rouges is more subdued and Alpine deformation is documented by the doming of the Triasic unconformity.

3.1 The roots of the Helvetic nappes in the Val Ferret.

To the east, the Swiss flank of the Mont-Blanc massif mostly corresponds to structural surfaces of Triassic sandstones lying unconformably on the granite (Fig. 2). Intensively sheared Mesozoic slates overlie the Triassic rocks. Within the slates, the schistosity strikes N22 65° SE on average and carries a well-defined stretching lineation striking N134 65° SE on average (Fig. 3c and Fig. 4a). The slates are affected by recumbent folds verging to the NW (Ayrton, 1969), consistent with shear criteria indicating a top to the NW sense of shear (Fig. 3d). In some places “a” type and sheath folds testify to the intensity of shearing along what we will call the Val Ferret thrust. Towards the south, this thrust becomes slightly oblique to the stratigraphy and affects the granite (Fig. 2 and Fig. 4a). Farther to the north, in the Mt Chemin area, 5 km south-east of Martigny, thrusting has occurred along the Triassic unconformity, and dismembered Permo-Triassic sediments form a sliver between the Variscan gneisses and the Mesozoic sheared rocks (Fig. 2a and Fig. 5a). Cartographically, the Val Ferret thrust continues to the north and, disappears beneath the thick Quaternary infill of the Rhône valley. North of that valley, the most probable equivalent of this thrust is the basal contact of the Morcles nappe (Fig. 2a).

3.2 The Mont-Blanc back-thrust.

Between the Mont-Blanc de Courmayeur and the Grandes Jorasses the southwestern flank of the range is impressively steep (average slope of 35° from the top of the Mont-Blanc de Courmayeur to the Val Veni over 3000m below). It is marked by several steeply northward dipping thrust-faults (Fig. 2a). The southernmost thrust brings the Mont-Blanc granite on top of the Jurassic-Cretaceous sedimentary series (e.g., Baggio, 1964; Antoine et al., 1975; Guermani and Pennacchioni, 1998). North-east of Courmayeur, near Pra Sec, the thrust dips 55° to the NW (Pr on Fig. 6), is marked by a ~2m thick fault breccia and brings the granite on top of black schists and Cretaceous sandy limestones that were previously interpreted as lying unconformably on the granite (Antoine et al; 1975; 1979). Farther SW, below the Boccalatte refuge and near the Mont Fretty the contact dips 50 to 65° to the NW and brings the granite on top of overturned Liassic slates. These series probably correspond to the roots of the Helvetic nappes in the hanging wall of the Val Ferret thrust, but overturned below a counter thrust: the Mont-Blanc back-thrust (Fig. 2). The contact is well exposed on the trail to the Boccalatte refuge where it corresponds to a ~50 meters thick granite cataclasite layer (Fig. 3e). West of Mont Fretty, within the granite numerous greenschist shear zones anastomose around less deformed lenses (Guermani and Pennacchioni, 1998). Most mylonitic shear zones trend N16 to N52 and display shear criteria suggesting top to the SE (dip-slip) thrusting. However, given the common absence of stretching lineations and the strong influence of pre-existing brittle faults on the shear zones geometry (Guermani and Pennacchioni, 1998), the precise direction of thrusting is difficult to constrain. The brittle faults that affect the granite show chlorite crystallisation, are mostly parallel to the Mont-Blanc back-thrust and often show dip slip motions (Fig. 6). Northwest of Courmayeur, near Peuterey village, the fault contact strikes N36, is nearly vertical (P on Fig. 6), and shows evidence for upward motion of the northwestern (Mont-Blanc) unit. Within the granite, ~2 km away from the main contact, two major shear zones straddle the Aiguille de la Brenva (Fig. 2a) and probably merge at depth to form the major NW dipping shear zone found in the Mont-Blanc tunnel 3.5 kilometers from the Italian entrance. The northernmost shear zone outcrops near the Helbronner cablecar station and exhibits a clear morphological trace through the Peuterey and Rey passes, at the base of the highest part of the Mont-Blanc massif (Fig. 2a). In the deformed sedimentary series of the Val Veni, few brittle faults that reactivate schistosity planes show dextral motion (Fig. 6).

3.3 The Mont-Blanc shear zone (MBsz).

The northwestern flank of the Mont-Blanc massif corresponds to the edge of the Chamonix valley deeply carved by the glaciers within the stripe of Mesozoic sediments pinched between the Mont-Blanc and the Aiguilles Rouges. These sediments are deformed and locally overturned below the Mont-Blanc granite and the Variscan gneisses (Fig. 5e). Early workers interpreted this geometry as indicative of Alpine thrusting of the Mont-Blanc basement on top of the Mesozoic series and of the Aiguilles Rouges massif (e.g., Bellière, 1956; Eltchaninoff-Lancelot et al., 1982; Buttler, 1985; Gourlay, 1986). Within the Mont-Blanc basement rocks, the contact is marked by an up to 4km wide zone of heterogeneously deformed mylonitic rocks, interpreted as due to Tertiary thrusting of the Mont-Blanc (Bellière, 1956). However, the same author later claimed that the mylonites were locally intruded by the Variscan Mont-Blanc granite and unconformably covered by Mesozoic sediments (Bellière, 1988). He thus restricted the alpine deformation to a single brittle fault named the "Faille d'Angle" (Fig. 2a). For others, the contact between the Mont-Blanc basement and the Mesozoic series is an overturned unconformity (e.g., Epard, 1986). Our study refutes these later views and confirms the existence of a Tertiary reverse shear zone fringing the Mont-Blanc to the NW: the Mont-Blanc shear zone (MBsz, Fig. 2 and Fig. 5). If it is true that the Mont-Blanc granite and related dykes intrude Variscan metamorphic rocks, all these rocks are deformed in the MBsz that we describe in more details below.

From Sembrancher (NE) to the Jovet pass (SW), the MBsz is marked by SE-dipping greenschist foliations that affect the Mont-Blanc granite and overprint the variscan schists. This deformation was characterized in the field along 12 cross sections; five of these sections are taken to illustrate the overall strucuture (Fig. 5). The green-schist foliation is marked by white micas, chloritized biotites and chlorite (Fig. 3j). The foliation anastomoses around boudins of variscan gneisses free of any green-schist deformation. Within these boudins, aplitic dykes, similar to those found in the Mont-Blanc granite, crosscut the variscan age foliation (Fig. 3b), while outside of the boudins, the dykes are affected by the mylonitic deformation (Fig. 3h). Around the boudins, the green-schist foliation trends N355 to N80 (N35 48 E on average; Fig. 4d), and bears a steep mineral and stretching lineation with pitches between 90° to 70° NE (average direction: N110 50E; Fig. 3g and Fig. 4d). Shear criteria in the mylonites (mostly S/C relationships), consistantly indicate a top to the NW (thrusting) sense of shear (Figs. 3h, 3i and 3j). Near Le Tour, the Mesozoic sediments that structurally underlie the Mont-Blanc gneisses (Fig. 5c) show schistosities and a stretching lineation (e.g. ME45, schistosity 24E60, lineation pitch 78N) parallel to the gneissic mylonites (Fig. 4c & d). C/S relationships within these rocks clearly indicate thrusting (Fig. 3f). These field relationships imply that the greenschist metamorphism and deformation of the NW border of the Mont-Blanc massif is of Alpine age. The kinematics of that deformation implies that the MBsz is a steep reverse ductile fault with a minor dextral component of movement.

Towards the southwestern end of the Mont-Blanc massif, the greenschist foliation tends to be shallower and exhibits less clear lineations. At the Col de Tricot, the Mesozoic sedimentary rocks just below the basement gneisses are mylonitic and show shear planes with white mica neocrystalisation. These mylonites are sub-parallel to the green-schist foliation in the overlying basement gneisses and to the axial-plane cleavage in the underlying Mesozoic rocks (Fig. 5, section 8) (e.g. Belière, 1956). This relationship indicates alpine thrusting of the Mont-Blanc basement on top of the Mesozoic sediments of the "Chamonix syncline" contrary to the conclusions of Epard (1986), who advocated for an inverted unconformity.

3.4 Deformation within the Mont-Blanc granite

Within the Mont-Blanc granite, the preferred orientation of biotites, sometimes feldspars, and of restitic enclaves, marks a sub-vertical magmatic foliation striking NNE-SSW (Von Raumer, 1967). Aplitic veins cut this foliation. Both the granite and the aplitic veins are affected by numerous green-schist shear zones and faults that post-date the magmatic foliation. Shear zone mylonites bear muscovite + green biotite + albite + chlorite ± epidote ± titanite (Rolland et al., 2003) while the faults show either chlorite or epidote fiber crystallisations. The faults and shear zones have a large range of orientations but most trends NW-SE with an inverted fan geometry across the range. They are generally parallel to the MBsz to the NW and to the Mont-Blanc back-thrust to the SE (Bertini et al.; 1985), (Fig. 2b). The granite is also affected by numerous horizontal tension gashes and veins filled with quartz crystallisations. These veins when open yield spectacular automorphic quartz crystals, they may also contain epidote, K-feldspar (adularia), fluorite, muscovite and calcite.

3.5 The Aiguilles Rouges massif.

The Aiguilles Rouges massif is mostly composed of Variscan gneisses and micaschists. A few granites, such as the 306±1.5 Ma Vallorcine granite (Bussy et al., 2001), intrude these rocks. Foliations are generally steep, strike N335° to N55° (N20° on average, Fig. 4b) and are locally affected by isoclinal folds. When present, the lineation dips relatively shallowly, 22 to 55° to the N (Fig. 4b). The Aiguilles Rouges also includes Late Carboniferous basins affected by Late Variscan deformations (Fig. 2a). Triassic conglomerates and sandstones unconformably cover these basins as well as the metamorphic and granitic rocks (Fig. 2a).

The intensity of alpine deformation can be estimated by looking at the present day geometry of the Triassic unconformity that describes a broad NE-SW dome (Fig. 2b). The unconformity is mapped as horizontal at an elevation of ~2850m, below the summit of the Aiguille de Belvédère (Fig. 2a); (Bellière et al.; 1987), while on the northwestern flank of the Aiguilles Rouges it dips ~30°NW and is overlain by the Liassic décollement zone (for instance near the Anterne and Emosson lakes). Farther NW, it is found at an elevation of 1200m NE of Sixt (Fig. 2, Pairis et al., 1993). Outcrop-scale observations (for instance above the Vieux Emossons lake) suggest that warping and small-scale folding of the unconformity is accommodated by distributed slip on the pre-existing steep foliation planes in the basement rocks. Above the unconformity, the Liassic décollement zone fringes the whole northwestern flank of the Aiguilles Rouges massif and merges with the reverse limb of the Dent de Morcles recumbent fold, basal contact of the Helvetic nappe stack (Fig. 2a). The entire Helvetic nappe stack has the same domal shape as the underlying Triassic unconformity (e.g., Pfiffner et al., 1993).

3.6 Summary and relative chronology of Alpine deformations in the Mont-Blanc–Aiguilles Rouges area.

The first major Alpine deformation in the Mont-Blanc area is the formation of the Penninic nappes above the Penninic basal thrust that ended in the Upper Eocene (e.g., Pfiffner et al., 2002); (A on Fig. 2b). The structural observations presented above shed light on more recent deformation events in the footwall of the Penninic basal thrust.

The geometry of the Subalpine chain, the Helvetic nappes and the location of their roots, as well as the importance of NW-vergent alpine thrusting of the Mont-Blanc has been the subject of a lively debate. Mont-Blanc thrusting is of major importance for some (e.g., ~50 km for Ayrton, 1980 or more than 67 km for Butler, 1985), while it is nonexistent for others (e.g., Epard, 1986; Gidon 2001). The roots of the Helvetic nappes have been placed in the Chamonix synclinorium (Ayrton, 1980; Eltchaninoff-Lancelot et al., 1982), within the Mont-Blanc massif itself between an internal and an external Mont-Blanc (e.g., Epard, 1990) or in the Val Ferret east of the Mont-Blanc. Our structural observations show that the so-called "external" Mont-Blanc corresponds to the Mt-Blanc shear zone (MBsz). This steep reverse fault offsets the basal contact of the Sub-Alpine and Helvetic nappes (Fig. 2b). In our interpretation, this contact, the basal contact of the Mesozoic sediments in the Chamonix synclinorium and the Val Ferret thrust, all correspond to the same major thrust: the Helvetic basal décollement (HBD), rooted east of the Mont-Blanc. The HBD is refolded in a broad anticline above the Aiguilles Rouges and Mont-Blanc basement culmination and is offset by the MBsz (Fig. 2b). Deformations observed in the Mesozoic sediments of the Chamonix valley are thus related to two distinct structures: the HBD and, the MBsz (Fig. 4c).

This implies that both the doming and uplift of the Aiguilles Rouges – Mont-Blanc culmination (C on Fig. 2b) and the initiation of the MBsz (D on figure 2b) took place after over-thrusting of the Helvetic nappes (B on Fig. 2b). However, the relative timing between the doming and the MBsz remains unclear. We favour a scenario with doming of the Aiguilles Rouges taking place first, before out-of-sequence activation of the MBsz (figure 2). Alternatively, the MBsz could have been active first, followed by propagation of deformation on a lower angle fault towards the NW. In that case, the MBsz would have been transported passively toward the NW.

Along the southern extremity of the Mt-Blanc, the Pennaz imbricates involve steeply-dipping slices of deformed Mesozoic sediments. In that area, basement rocks of the Roselette klippe rest on top of Mesozoic sediments NW of the Pennaz imbricates. This geometry led Butler (1983) to propose a NW-vergent flat thrust of the Mt-Blanc. In a comment on Butler's (1983) work, Platt (1984) proposed the existence of a late steep fault, termed "breach thrust". Our observations are more in accordance with Platt's (1984) interpretation, with the Roselette klippe corresponding to a piece of basement rock involved within the HBD, latter cut by steep faults In the southern prolongation of the MBsz (Fig. 2). In most areas of the Mont-Blanc and Aiguilles Rouges massifs, the HBD sits just above the Triassic unconformity, but in other places it clearly cuts off basement rocks, as observed along the southern portion of the Val Ferret Thrust (Fig. 2a). Such local involvement of the basement in the décollement level probably results from the existence of tilted blocks inherited from Mesozoic extension. The Pennaz inbricates that contain basement slices are thus probably steepened traces of the Helvetic décollement, partly reactivated by splays of the MBsz.

Within the Mont-Blanc granite, the crystallized gashes, and the post-magmatic shear zones, interpreted by all authors to be of Alpine age, are compatible with a ~NW-SE compressive stress with σ3 vertical. The detailed interpretation of the brittle faults is more complex. On both sides of the Mont-Blanc, most brittle faults show dip-slip motion. These faults are most probably conjugate faults, implying a NNW-SSE maximum horizontal stress (σhmax) striking between N134 and N176 (Fig. 6). These faults are parallel to the Mont-Blanc back-thrust (Fig. 6), which thus appears to have formed under a NNW-SSE compressive stress-regime. However, such compression would induce a reverse/sinistral motion on any NE-SW plane, and cannot explain the reactivation of few cleavage planes in dextral faults south of the Mont-Blanc, nor the transport direction on the MBsz, which has a significant right-lateral component (Fig. 6). It is thus very likely that at least two distinct directions of compression were present during the late evolution of the Mont-Blanc massif: one oriented WNW-ESE during motion along the MBsz (D on Fig. 2), and another oriented NNW-SSE during motion along the back-thrust (E on Fig. 2). The back-thrust is probably the most recent of the two structures because: a) deformation on the backthrust is largely brittle suggesting an activation at a time when the granite had already been partly exhumed; b) at the "Nid d'aigle" on the northern flank of the Mont-Blanc, the brittle faults conjugated with the Mont-Blanc back-thrust are late with respect to the MBsz schistosity; and c) the slope of the S flank of the range is exceptionally steep, even more than the north flank, suggesting recent and possibly still active uplift.

4 Constrains on the amount and timing of alpine metamorphism and External crystalline massifs exhumation.

4.1 Variscan and Alpine metamorphisms.

The Aiguilles Rouges and the Mont-Blanc massifs experienced at least two metamorphic phases: during the Variscan and the Alpine orogeny. After Variscan metamorphism and granitic intrusions, portions of both massifs were exposed at the surface prior to the deposition of Triassic sandstones.

In the Aiguilles Rouges massif, a large part of the exhumation occurred before the deposition of Late Carboniferous (308-293 Ma) clastic and coal-bearing sediments (Capuzzo and Bussy, 1999, Capuzzo et al., 2003). Variscan P-T paths show high-pressure metamorphic conditions: up to 12kb (Von Raumer et al., 1999). In contrast, Alpine metamorphism is limited to the zeolite facies: pumpellyite-phrenite-clorite-titanite-albite-calcite-Kfeldspar (Von Raumer, 1974). Based on illite crystallinity, alpine metamorphism at the base of the Helvetic nappes, and thus at the top of Aiguilles-Rouges and Mont-Blanc basement, belongs to the epizone (≥300°C) (Aprahamian, 1988). This is confirmed by $\delta^{18}O$ measurements in syntectonic veins of the Morcles nappe suggesting temperatures of 350±20°C at the beginning of the deformation (Fig. 7) with a slight decrease of temperature (30 to 50°C) during deformation (Kirschner et al., 1995).

In the Mont-Blanc, the only P-T data attributed to the Variscan metamorphic episode comes from its NE extremity, and indicate isobaric cooling at medium pressure and temperatures (6±1 Kb and 550±40 to 450±50°C; Marshall et al., 1997). The Mont-Blanc granite emplacement depth has been estimated as between 4 and 14 km (1 to 3.8 Kb); (Marshall et al., 1997; Bussy, 1990). The occurrence of microgranular facies, and rhyolites on the NE flank of the massif underneath the Triassic unconformity (Bonin et al., 1993; Bussy et al., 2000) show that at least this part of the massif was exhumed prior to the Triassic. However, alpine metamorphism was stronger in the Mont-Blanc than in the Aiguilles Rouges. It induced crystallisation of green-schist minerals: actinote, green biotite, chlorite, epidote, albite and titanite, and more locally, Hornblende, Zoïsite, Clino-zoïsite and white mica (Von Raumer, 1974). White micas crystallised in shear planes of Alpine mylonites that deform the Variscan gneisses, the Mont-Blanc granite and the Mesozoic cover rocks. Within the granite, Mucovite-Chlorite equilibria in a muscovite+biotite+chlorite+epidote bearing shear zone gives P-T estimates of 0.5±0.05 GPa and 400±25°C (Rolland et al., 2003); (10, Fig. 7). Alpine P-T conditions are also constrained by micro-thermometric studies of fluid inclusions within minerals (mostly quartz) hosted by alpine veins (1 to 9, Fig. 7) (Poty et al., 1974; Poty and Cathelineau, 1999; Fabre et al., 2002; Marshall et al., 1998b). All of the P-T estimates are combined in Figure 7 to define the alpine exhumation path of the Mont-Blanc rocks. The temperatures culminate at ~400°C, in good agreement with estimates from the base of the Morcles nappe (Fig. 7).

4. 2 Existing geochronological constrains.

Two $^{40}Ar/^{39}Ar$ hornblende ages (≥334 and 309±6 Ma) at the northeastern extremity of the Mont-Blanc have been interpreted as maximum ages for the Variscan metamorphism, probably linked with granite emplacement (Marshall et al., 1997). The ages of the Mont-Blanc granite itself (303±2Ma; Bussy and Von Raumer, 1993) and of several magmatic and anatectic rocks of the Aiguilles Rouges (between 332 and 306 Ma) are well constrained by U-Pb ages on zircons and monazites (Bussy et al., 2001).

Within the Mont Blanc granite, Baggio et al. (1967) were the first to describe and date secondary biotite crystallisation, mostly from shear zones. Their Rb/Sr ages span between 18 and 36 Ma (Fig. 8) but, because initial Sr values were assumed to be that of the whole rock analysis (Sr_i = 0.726), these ages are disputable. However, they reveal alpine recrystalization and/or strong reheating. Another approach has been K/Ar dating of adularia K-feldspar and muscovite within the alpine veins. Ages range from 15.2 to 18.3 for adularia and 13.4 to 15.2 for muscovite (Leutwein et al., 1970) (Fig. 8). The corresponding Rb/Sr ages are anomalously old for adularia while a muscovite gives 14.8 Ma (Leutwein et al., 1970). A muscovite from a gold-bearing quartz vein shows excess argon and yields a 9.9±1 Ma $^{40}Ar/^{39}Ar$ isochron age (Marshall et al., 1998a). This suggests that most K/Ar ages from vein minerals are maximum ages. Muscovites and microcline from two different mylonites yielded 40±3 Ma (Leutwein et al., 1970) and 41±1 Ma (Krummenacher and Evernden, 1960) K/Ar ages respectively, almost identical to the 46.5±1.9 Ma $^{40}Ar/^{39}Ar$ age from paragonites of paragonite-keratophyre schists in Northeastern Mont-Blanc (Marshall et al., 1998b). This large distribution in age, revealing either multiple events or disequilibria in the chronometric systems, and the evidence for massive fluid circulation during the alpine deformation (e.g., Rolland et al., 2003, Rossi et al., in press), suggests that additional $^{40}Ar/^{39}Ar$ data would be useful.

The age of the Subalpine (Helvetic) nappe stack emplacement (event B, Fig. 2b) appears to be well constrained between 32 and ~15 Ma (Fig. 8). The Taveyannaz volcaniclastic sandstones that were deposited prior to the nappe stacking contain 32.5 Ma andesitic clasts ($^{40}Ar/^{39}Ar$ on hornblendes), while biostratigaphic correlations suggest sedimentation between ~32 and 29 Ma (Ruffini et al., 1995). Fine-grained synkinematic white micas (2 to 6 microns) from ductile mylonites at the base of the Morcles and Doldenhorm nappes show staircase $^{40}Ar/^{39}Ar$ age spectra between 13 and 76 Ma (Kirschner et al., 1996). 94% of the gas release show ages between 13 and 32 Ma that Kirschner et al. (1996) interpret as crystallization ages and thus as the duration of the nappe stacking. Such timing is confirmed by two independent studies. Small white micas (<2 microns) from a post tectonic vein within the Morcles nappe yield a K/Ar age of ~15 Ma (Huon et al., 1994). White mica within deformed Mesozoic sediments from the Val Ferret thrust, (~5 km north of Orsières, Fig. 2a) yield $^{40}Ar/^{39}Ar$ ages that young towards the fault (Crespo-Blanc et al., 1995). Of these young ages of 14.6±0.2, 15.5±0.4 and 18.5±0.2, Crespo-Blanc et al. (1995) retain the 15.5 Ma age from the thrust surface as indicative of the end of motion.

Apatites fission-track ages span from 3.1 to 4.2 Ma in the Aiguilles Rouges, and from 1.4 to 7.5 in the Mont-Blanc while most zircon fission-track ages span from 11.2 to 15.7 in the Mont-Blanc (Seward and Mancktelow; 1994; Soom, 1990; Carpéna, 1992) (Fig. 8). According to Seward and Mancktelow (1994), age and elevation are not correlated, however most samples were collected along roads or at low altitude with the exception of four samples within the Mont-Blanc massif that yield relatively old ages (Soom, 1990). According to Carpéna (1992), zircons from the Mont-Blanc tunnel and the Aiguille du Midi show a wide fission-track age spectra: from 10.8±4.6 to 32.8±0.7 with three age clusters depending on their typology and their U content (Fig. 8). Surprisingly, the younger ages are similar to the apatite ages while the older ones are more than 4Ma older than all other available fission-track data (Fig. 8). We will thus not consider these two extreme zircon fission-track age groups in our interpretation. When plotted together, fission-track ages of all ECM (Aar, Belledone, Mont-Blanc) show a broad correlation with respect to altitude, with a lower slope for zircons than for apatites, an observation that was used to infer an increase of the exhumation rate at ca 10Ma (e.g. Fügenschuh and Schmid, 2003).

4.3 New $^{40}Ar/^{39}Ar$ data.

In order to constrain the medium temperature thermal history of the Mont-Blanc massif, biotites and K-feldspars from samples of various lithology have been analysed (Fig. 9, Table1). Separation and analytic techniques are presented in appendix 1.

4.3.1 Biotites

Biotites from granite samples C2 (Helbroner) and C8 (Plan de l'Aiguille) show good plateau ages at 22.8±0.6 Ma and 22.4±0.1 Ma, respectively, with more than 65% of ^{39}Ar release (Fig. 10a, b). However, sample C8 has a saddle shape age spectrum, suggesting excess argon. An inverse isochron age of 16.6 ± 0.7 Ma is proposed for this sample (Table1, Fig. 8).

Biotites from samples C1 (granite, Aiguille du Midi) and ME25 (orthogneiss, Plan de l'Aiguille) show good plateaus with more than 85% of total ^{39}Ar released, with ages of 39.2±1.0 Ma and 63.0±1.2 Ma (Fig. 10a, b). Sample ME50 (granite, La Neuve) shows a disturbed age spectra; a mixed phase obviously degassed during the first heating steps, yielding meaningless old ages. The other steps give a reasonable plateau age of 63.7 ± 2 Ma using 40% of ^{39}Ar released (Fig. 10b).

All ages are much younger than the Paleozoic granite emplacement ages, although most of these samples contain minerals that did not experience strong alpine deformation (Table 1). The biotites thus appear to have been reset by at least one alpine thermal event. There are two distinct age groups: around 20Ma (C2 and C8) and around 63 Ma (ME25 and ME 50); (Table1, Fig. 8). C1 yields an intermediate age between the two groups, as do a paragonite sample (Marshall et al., 1998b). These groups are independent of the location and lithology: C2 and C8 come from opposite flanks of the Mont-Blanc, as do ME50 and ME25 (Fig. 9a).

4.3.2 K-feldspars

To further constrain the Alpine cooling history, several K-Feldspars have been analysed (Fig. 10, Table 1). Unfortunately, all feldspars from the Mont-Blanc massif yield complicated age spectra that prohibit any reasonable thermal modelling.

The initial parts of the age spectra, comprising up to 15% of gas release and corresponding to furnace temperature below 700°C, are the most disturbed, showing alternatively old and young ages (Fig. 10c, e, g). This is because our heating schedule systematically duplicated the degassing steps; this often results in the second step of every pair having a younger age (c.f. Harrison et al., 1994). In the first part of the age spectra, the ages are correlated with the $^{38}Ar/^{39}Ar$ isotopic ratios (Fig. 10d, f, h), which can be used as a proxy for the Cl/K ratio. The old ages thus probably correspond to the degassing of Cl rich inclusions containing excess argon, while the young ages are almost free of excess argon (Harrison et al., 1994).

At around 20% of gas release, most age spectra show a bump in age (Fig. 10c, e, g). Subsequently, the $^{39}Ar/^{37}Ar$ ratio, proxy for the K/Ca ratio, tends to increase (Fig. 10d, f, h). This suggests a mineralogical change in the degassing feldspar towards more pure orthoclase. After this bump, some spectra show a small age plateau (Fig. 10c, g) indicating a medium temperature age (Kf MT average age, Fig. 8, Table 1). Ages corresponding to higher furnace temperatures (1000-1200°C) increase (Kf HT maximum age, Table 1).

Two hypotheses can explain both the general shape of the age spectrum and the corresponding chemical zoning. The first explanation is that degassing of Variscan zoned K-feldspar produced this pattern. The second possibility is that recrystallised rims around inherited Variscan K-rich cores, yielded the first and second parts of the age spectrum, respectively. In both hypotheses, the K-feldspar would have been strongly reset during a Cenozoic thermal event, creating the second part of the age spectrum. In the first hypothesis, the initial part of the age spectrum would correspond to the final cooling recorded by the K-feldspar (around 150°C), while in the second hypothesis it would correspond to the age of feldspar recrystallisation. We favour that second hypothesis given the widespread occurrence of secondary K-feldspar crystallisation in the Alpine veins (adularia) and surrounding rocks of the Mont Blanc massif (e.g., Rossi et al., in press). In the Aiguilles Rouges massif, the K-feldspar core was not completely reset and the sample shows a Variscan (≥300 Ma) HT maximum age (ME30, Table 1). On the other hand, in the Mont-Blanc massif all feldspars have HT maximum ages less than 110Ma; eight of the ten samples yield Tertiary ages (Table 1). This indicates that the thermal event reached temperatures close to 400°C, in good agreement with the P-T path (Fig. 7). In this context, the medium temperature (MT) plateau ages probably correspond to an episode of rapid cooling. The clearest MT plateaus are found in the alpine mylonites and are between 22 and 13 Ma (Fig. 8). We thus suggest that significant cooling from temperatures around 400°C took place in the Mont-Blanc massif during this time interval. This would be in good agreement with biotites ages from samples C2 and C8 (Fig. 8). Biotite ages are usually considered to reflect cooling below 320±40°C (e. g., Harrison and Amstrong, 1978; Leloup et al., 2001).

The age of the feldspar overgrowth (or the last cooling episode) is difficult to calculate precisely due to the presence of excess argon in the first part of the age spectra. Because of this excess argon, the lowest age (Kf LT minimum age, Table 1) is most significant, and is probably the best estimate for the age of the feldspar overgrowth. Sometimes some of the duplicate steps define a low temperature plateau (Fig. 10c, e, g). However, these younger steps could also be affected by excess argon, as suggested by inverse isochron ages (Kf LT isochron, Table 1). The Kf LT minimum age is thus considered as a maximum age for the K-feldspar overgrowth (Fig. 8). Within the Mont-Blanc massif, all K-feldspars have LT minimum ages younger than 18 Ma (Fig. 8, Table1). Of these 10 samples, only two (ME37 and C1) are older than 16 Ma while all other samples yield ages between 7 and 11 Ma (Fig. 8). ME 30 from the Aiguilles Rouges yields an older, but still Tertiary, LT age (27 Ma). As stated above, this is a maximum age, and a 12±2 Ma isochron age can be proposed instead (Table 1). Such an age would be in better agreement with the 17 Ma zircon fission-track age from the same massif (Soom, 1990), as well as Kf LT ages of 12 and 14 Ma obtained respectively in the Belledonne and Aar massifs (Table 1, Fig. 8).

4.4 New apatite fission-track data.

In order to constrain the lower part of the cooling history, 8 new apatite fission-track ages have been obtained (Fig. 11, Table 2). Most samples lie along a NW-SE section through the Aiguilles Rouges and Mont-Blanc massifs, with samples collected between ~1000m high in the Chamonix valley and the Mont-Blanc tunnel, and 3800m on the Aiguille du Midi (section 6, Fig. 2a and Fig. 9). ME144 is slightly offset from cross-section 6, coming from the highest outcrop: above the Col Major at 4760 m of altitude. The fission-track methodology is presented in appendix 2.

All ages lie between 2.7±0.5 and 5.0±0.6 Ma (Fig. 8, Table 1), in the same range as previously published ages (Fig. 8). Due to the young ages, confined track lengths could not be measured. The highest samples tend to show the oldest ages, but the correlation is difficult to quantify, partly because the uncertainties on the ages are relatively large (Fig. 11a1)s.

5 Discussion.

The high altitude of outcroping basement rocks in the Mont-Blanc and the young apatite fission-tracks cooling ages suggest a significant amount of recent rock uplift and exhumation. As will be discussed below, structural studies indicate that uplift occurred by at least three distinct mechanisms: broad doming, reverse / dextral motion along the MBsz and reverse motion along the Mont-Blanc back-thrust (phases C, D and E; Fig. 2a). As the maximum pressure clearly documented for Alpine times is 5±0.5 Kb (Fig. 7), the total amount of exhumation is on the order of 20 km. The vast majority of the medium to low-temperature geochronological data are Neogene in age (Fig. 8), indicating that exhumation of the Mont-Blanc and Aiguilles Rouges took place during this interval. However the precise exhumation amounts and timings remain to be deciphered and are discussed below.

5.1 Amount of motion along the Chamonix shear zone and the Mont-Blanc back-thrust.

Prior to final exhumation, the Aiguilles Rouges and the Mont-Blanc were overthrust by the package of the Helvetic and PréAlpes nappes along the HBD (B, Fig. 2b); most of these nappes have subsequently been eroded away. The total thickness of the nappe package is estimated to be more than 6km (thickness of the Morcles nappe alone) and up to 12 km, based on classical cross-sections (Esher et al., 1988; Esher et al., 1993; Pfiffner, 1993). Prior to ECM exhumation, the depth and temperature of the Triassic unconformity and the HBD were approximately the same above the Mont-Blanc and the Aiguilles Rouges. In the Morcles nappe, temperature estimates from the HBD (350±20°C, Kirschner et al., 1995) are similar to those suggested by the upper bound of the alpine grade of metamorphism within the Aiguilles-Rouges basement. On figure 7, such temperatures correspond to 6–12 km depth, in good agreement with the estimated thickness of the nappe package. In the Aiguilles Rouges, the Triassic unconformity now outcrops at 2800m a.s.l. (Aiguille du Belvédère, Fig. 2a), corresponding to

~5 km more uplift than 25 km farther NW (Fig. 2b). A point now located at the top of the Aiguilles Rouges had thus been buried beneath ~9±3 km of Mesozoic rocks before being uplifted by a total of ~12±3km (eroded Mesozoic plus present day altitude) during the Neogene (C, Fig. 2b).

The Triassic unconformity is only preserved at the SE and NW extremities of the Mont-Blanc and has been completely eroded above the Mont-Blanc summit (~4800m a.s.l.) (Fig. 2a). This implies a minimum of 2000 m of differential uplift between the Mont-Blanc and the Aiguilles Rouges across the MBsz (D, Fig. 2b). The observation that the Triassic unconformity describes a broad antiform and must underlie the Mesozoic sediments of the Chamonix valley at ~1000m a.s.l. raises the minimum differential uplift to ~4 km. This value leads to a total exhumation of ~16±3 km for the Mont-Blanc rocks, in good agreement with several fluid inclusion P-T estimates (2, 4, 8, Fig. 7). The 5±0.5 Kb pressure estimate of Rolland et al. (2003) implies an even deeper alpine origin for the Mont-Blanc rocks (~20 km) and thus a larger differential uplift (~8 km) across the MBsz (Fig. 7).

The amount of exhumation clearly varies both along and across strike of the Mont-Blanc. For example, in the NE Mont-Blanc, the Triassic unconformity is widely exposed, and exhumation has been limited to the thickness of the overlying nappes (9±3 km). The unconformity dips 60 to 70° to the east. Assuming that the unconformity was initially horizontal and that the 8 to 14 km wide massif was rigidly tilted leads to 7-13 km more uplift along the western flank of the massif than along the eastern one, and thus to a total exhumation of 13-25 km in the west. This is in good agreement with the pressure estimates from Rolland's et al. (2003).

Along strike the level of erosion is clearly shallower SW and NE of the Mont-Blanc, where the Helvetic nappes are preserved. Furthermore, the deepest erosion levels correspond to the highest elevations. This implies an important spatial variation in the total exhumation. A straightforward interpretation is that the throw on the MBsz dies out SW and NE of the Mont-Blanc with maximum offsets between Chamonix and l'Argentiere. One may note that in the footwall of the MBsz, exhumation variations in the Aiguilles Rouges mimics but are smaller than in the Mont-Blanc.

A more detailed look at the topography highlight another mechanism. Elevation decreases abruptly SW of the summit of the Mont-Blanc and more gradually towards the NE. Elevations exceeding 4000m are located almost exclusively in the hanging wall of the Mont-Blanc back-thrust, from the Grandes Jorasses to the Mont-Blanc itself. The latter is located where the Mont-Blanc back-thrust meets the MBsz (Fig. 2a) suggesting that the highest altitudes result from the interaction of these two structures. We suggest that altitudes reached a maximum of 4000m in the hanging wall of the MBsz (Aiguille Verte), while the exceptional altitude of the Mont-Blanc is due to further motion on the Mont-Blanc back-thrust (E, Fig. 2b) that added ~1 km of uplift.

5.2 Timing of deformation phases.

Until now, timing of exhumation of the ECM has been exclusively discussed on the light of fission-track data (e.g. Seward and Mancktelow, 1994). Our new geochronologic data provides a broader perspective for establishing the absolute timing of the tectonic phases discussed in section 3.6. With the exception of U/Pb ages that correspond to the timing of Variscan deformation and granite emplacement (~300 Ma), all of our data are Tertiary in age, mostly distributed between 22 and 2 Ma. Only six analyses yield much older ages between 40 and 64 Ma (Fig. 8). Structural relationships imply that uplift and exhumation of the Aiguilles Rouges and Mont-Blanc postdates most of the motion on the HBD, which ended around 15Ma (Huon et al., 1994; Kirschner, 1996; Crespo-Blanc et al., 1995), (Fig. 8). The simplest interpretation is thus that most of the rock uplift of the Mont-Blanc took place since 22-15 Ma, while older ages likely correspond to previous thermal or tectonic events.

5.2.1 Neogene exhumation of the External crystalline massifs.

Due to the complexity of $^{40}Ar/^{39}Ar$ K-feldspar spectra and the relative spread of the other argon and Rb/Sr ages between 22 and 9 Ma, detailed interpretation of the geochronological data is not straightforward.

We interpret the biotite minimum Rb/Sr ages, the zircon fission-track ages and some of the $^{40}Ar/^{39}Ar$ ages (C2 and C8 biotites, ME41, ME27 and ME36 Kf MT average age) as reflecting cooling of the Mont-Blanc between ≥400 and ~300°C, between 22 and ~12 Ma. For biotites, the closure temperature is estimated at 320±40°C for the argon system, and 300 to 350°C for the Rb/Sr system (e. g., Harrison and Amstrong, 1978). Such temperatures are compatible with the K-feldspar argon closure temperature, as well as high values for zircon fission-track closure temperatures (250±50°C; Hurford, 1986). This cooling would be concomitant with the crystallisation of muscovite and K-feldspar in the alpine veins (18.3-13.4 K/Ar and Rb/Sr ages, Fig. 8). Compared with the Mont-Blanc average P-T path, such cooling would correspond to 8 to 14 km of exhumation depending on the pressure estimate considered as a starting point for the uplift history (2 or 11, Fig. 7).

The young $^{40}Ar/^{39}Ar$ ages (Kf-LT minimum ages) are mostly between 11 and 6 Ma. These are interpreted as the age of feldspars overgrowths (see above), which probably formed around 150-200°C. The $^{40}Ar/^{39}Ar$ age of adularia crystallization in the most superficial alpine veins is within this age range (Fig. 7 and Fig. 8). That time interval could corresponds to ~5 km of exhumation of the Mont-Blanc (Fig. 7).

The few zircon fission-track and K-feldspar LT data from the Aiguilles Rouges are older than those from the Mont-Blanc. According to these data, the Aiguilles Rouges cooled below 300°C around 17Ma, ~4 Myr prior to Mont-Blanc (Fig. 8).

Cooling below 150-200°C occurred at ~12Ma, synchronously with the Belledonne massif but 1 to 4 Myr prior to the Mont-Blanc (Fig. 8).

All apatite FT ages are younger than 7.5 Ma (Table 2, Fig. 8 and Fig. 11a2). The apatite crystals have cooled from temperatures above their total annealing temperature (≤150°C, Ketcham *et al*., 1999) and record information on their cooling path during exhumation (e.g. Green *et al*., 1989a, 1989b). However, for such young apatites, it is difficult to obtain sufficient track-length measurements to permit robust thermal modelling. Given the evidence of rapid cooling, the data are thus simply taken to indicate the time at which the samples passed through the partial annealing zone (ca. 150-60°C). Given the young ages and their average uncertainty, typically ~0.5 Ma, precise calculation of exhumation rates is impossible. However, first order observations can be made. a) Along section 6, apatite fission-track ages on both sides of the Mont-Blanc shear zone at altitude below 1500m are ~4Ma (Fig. 11b). Thus it appears that there has been no significant differential unroofing between the two massifs since that time. b) On the other hand, ~5Ma old samples are located ~2000 m higher on the Mont-Blanc than on the Aiguilles Rouges (Fig. 11b). c) On a plot of age versus altitude, a correlation can tentatively be proposed with three distinct trends (Fig. 11a2): an exhumation rate of a few mm/yr before ~4 Ma, then a ca. 1.5 Myr period of slow exhumation, followed by a final pulse of rapid exhumation during the last ca. 2-3 Myr. This last phase of rapid cooling is inferred from the very young ages of some apatite (~2.5 Ma) implying an exhumation rate that can not be lower than 0.4mm/yr (Fig. 12a2) and is more probably ca. 1 mm/yr, as in the Aiguilles Rouges (Fig. 11a4). d) Along section 6, within the Mont-Blanc, the low altitude samples, mostly within the tunnel, tend to give younger ages toward the SE (Fig. 11b). This suggests more recent exhumation on the SE flank of the Mont-Blanc, probably along the back-thrust. However, no jump in age is detectable across that structure, probably because of the very young age of the samples (Fig. 11b). e) Along strike, younger apatite fission-track ages (~1.5 Ma) are observed at the NE end of the Mont-Blanc (Seward and Mancktelow, 1994). This may reflect lateral growth of the back-thrust

The data discussed above allow us to propose first order absolute time milestones along the global P-T path followed by the Mont-Blanc rocks (Fig. 7). However, given the uncertainty in age, temperature, and pressure, it is difficult to determine whether the exhumation rate, 0.8±2 mm/yr averaged over the last 22 Ma, actually varied significantly during this time. For example, following the global Mont-Blanc P-T curve, one can propose that between 22 and 12 Ma the cooling rate was 11°C/Ma, corresponding to an exhumation rate of ~1.4mm/yr, while from ~12 to ~6Ma the cooling rate increased to 28°C/Ma but corresponds to a lower exhumation rate of 0.8 mm/yr. However, such figures have large uncertainties and rest on a global P-T path that does not take sample location, advection or topographic affects into account.

5.2.2 Pre-Neogene geochronological data.

Data older than 40 Ma have to be interpreted with caution. The oldest $^{40}Ar/^{39}Ar$ biotite data (C1, ME25 and ME50), the paragonite $^{40}Ar/^{39}Ar$ data (Marshall et al., 1998a), the ~40 Ma mica K/Ar ages, as well as the oldest biotite Rb/Sr ages (Baggio et al., 1967), (Fig. 8), could be ascribed to a partial resetting of Variscan ages leading to spurious intermediate ages. However, in the case of the $^{40}Ar/^{39}Ar$ biotite ages, 1 Myr at ~400°C should be sufficient to completely reset the K/Ar isotopic system, and partial resetting should have produced less regular age spectra. Unfortunately inverse isochron plots for these samples are either unpublished or meaningless. The only exception is C1, which yields a 39.4 ± 1.3 Ma isochron age very close from the plateau age (Table1). Thus the existence of early tectono-thermal events around 63 Ma (ME25 and ME50), and between 40 to 50 Ma (C1, paragonite and K/Ar ages) cannot be totally excluded. Ages around 40 Ma could reflect Eocene underthrusting of the Mont-Blanc below the Penninic basal thrust, in accordance with stratigraphic constraints for the age of the Ultra Helvetic and Penninic nappes (e.g., Pfiffner et al., 2002) (A, Fig. 2b; Fig. 8; Fig. 12a,b). The geological interpretation of the 63 Ma data is more obscure. It is difficult to understand what event could have reset ME25 and ME50 biotites within the Mont-Blanc located far to the west from the deformation front at ~63 Ma (see Fig. 12a).

5.2.3 Proposed alpine P-T-t-D history of the Mont-Blanc massif.

Taking the previous discussion into account, we propose the following scenario for the Alpine structural evolution of the Mont-Blanc and Aiguilles Rouges.

1) In the Early Eocene, prior to alpine deformation, the Mont-Blanc and Aiguilles Rouges were buried below the Subalpine (Helvetic) sedimentary series (Fig. 12a).

2) During the Upper Eocene, the Versoyen and Valaisan series were thrust to the north along the Penninic décollement (Phase A, Fig. 2a, Fig. 8, Fig. 12b).

3) Between ~30 and ~15 Ma. thrusting took place along the HBD, bringing the Helvetic (Subalpine) nappes on top of the future ECM. At that time, deeper parts of the Mont-Blanc reached ~400°C and 14-20 km depth, while the upper part of the Aiguilles Rouges was at ~9 km depth and ~300°C (Phase B, Fig. 2a, Fig. 8, Fig. 12c, d).

4) Around 22 Ma, initiation of the alpine sole thrust induced uplift of the ECM with doming of the Aiguilles Rouges and tilting of the Mont-Blanc (Phase C Fig. 2a, Fig. 8, Fig. 12d).

5) At ~12Ma. movement on the MBsz induced relative vertical motion between the Aiguilles Rouges and Mont-Blanc. Uplift slowed down in the Aiguilles Rouges while it remained rapid in the Mont-Blanc, leading to 4 to 8 km of additional uplift (Phase D, Fig. 2a, Fig. 8, Fig. 12e,f).

6) Prior to ~4 Ma ago, motion on the MBsz shear zone stopped; subsequent exhumation results primarily from activation of the Mont-Blanc back-thrust, leading to the final elevation of the southern part of the Mont-Blanc massif (Phase E, Fig. 2a, Fig. 8, Fig. 12g). Apatite F-T data suggests that the Mont-Blanc back-thrust could have initiated ~2.5 Ma ago.

Figure 11 represents how such P-T-t-D evolution can be integrated in the structural evolution of the external Alps.

5.3 implications for the structural evolution of the Alps.

Northwest of the Mont-Blanc, the Jura is an arcuate fold belt created by thin-skinned tectonics above a décollement level in the Triassic evaporites (Fig. 1). NW of the Mont-Blanc, the Jura folds account for 20 to 28 km shortening in a NW-SE direction (Guellec et al., 1990, Affolter and Gratier, 2004). The Jura décollement can either root below the Aiguilles Rouges or be continuous with the HBD and root farther to the SE. A key point to distinguish between these two hypothesis is the timing of ECM uplift (e.g. Affolter, 2003). Deformations in the inner Jura started around 15 Ma ago (Beck et al., 1998, Deville et al., 1994) and propagated to the external Jura at 6±3Ma (Becker, 2000). Folding above the Jura décollement thus started when motion on the HBD stopped, at a time of important uplift in the ECM (Fig. 8, Fig. 12d, e). This strongly suggests that the Jura décollement does not root within the HBD, but rather that the ECM uplift was linked to the transfer of motion from the HBD to a deeper and more external thrust system: the alpine sole thrust (Fig. 12). The existence of such a thrust has been proposed by several authors (e.g., Ménard and Thouvenot, 1987; Butler, 1985; Lacassin et al., 1990) as the most probable cause for uplift of the Aiguilles Rouges and the Belledonne massif. Some SE dipping reflectors along the ECORS seismic line (C on Fig. 12h) could correspond to the trace of such thrust. However, the ECM are never clearly thrust above the sub-alpine sediments (e.g., Gidon, 2001). Our interpretation is that the basal thrust merged with the pre-existent HBD before propagating farther west below the Jura (Fig. 12d, e). The ECM are thus thrust upon the basement rather than the Mesozoic sediments (Fig. 2b), and form a backstop whose 20 to 28 km motion towards the NW since ~22 Ma induced the arcuate structure of the Jura.

Our study appears to confirm three successive stages (Penninic, Helvetic, Jura) of deformation, implying a ~100km long flat décollement in the external part of the orogen while deformation rooted in the more internal part (Fig. 12). Each décollement phase was active for 15 to 20 Myr and progressively stepped towards the foreland. This simple scenario of externally-vergent propagation was complicated by the ca. 12 Ma activation of the steep MBsz, which acted as an out of sequence thrust. While finite shortening above the Jura decollement strikes NW (Affolter and Gratier, 2004), perpendicular to the trend of the MBsz, that shear zone has a small dextral component. The geometry of the shear zone imply that 4 kilometre of vertical uplift of the Mont-Blanc would correspond to 5.5 km of throw on the fault, with 5.4 and 1 km of down-dip and right-lateral motion respectively. This corresponds to 3.7 km of horizontal shortening in the N110 direction. An 8 kilometres vertical motion would corresponds to 2.1 km of right-lateral motion for 7.5 km of shortening. The component of right-lateral shear might explain the few NE-SW dextral brittle faults observed (Fig. 6). Neogene NE-SW dextral faulting in the Mont-Blanc was first proposed by Gourlay (1983). Hubbard and Mancktelow (1992) later suggested an offset of 15 km, on a fault zone running along the Mont-Blanc massif and connecting the Simplon normal shear zone to the Pelvoux (Fig. 1). However, exposures of the corresponding structures are scarce, and the proposed offset disputable. If motion on the MBsz is indeed compatible with a NE-SW right-lateral transpressive regime, it accounts for less than a couple of kilometres of dextral motion between ~12 and ~4Ma. Alternatively, right-lateral shear could have taken place after the end of motion on the MBsz ~4Ma ago. Indeed, farther SW earthquake location and focal mechanisms suggest that the outer Belledonne massif (Fig. 1) is followed by a right-lateral seismic fault that could merge with the Chamonix Valley (Thouvenot et al., 2003). However, the strike of such fault is barely compatible with that of the Mont-Blanc back-thrust (see section 3.6). It follows that either the prolongation of the active Belledone fault is not along the Mont-Blanc; or that the Mont-Blanc back-thrust is now inactive. Given the very high altitude of the Mont-Blanc and the impressive morphology of its southern flank we favour the first hypothesis.

As the Aiguilles-Rouges and the Mont-Blanc massifs are separated by the Chamonix syncline, the other ECM are split along strike by a narrow band of Mesozoic rocks: the synclinal median between the internal and external Belledonne, and the Furka-Andermatt synclinorium between the Gothar and Aar massifs (Fig. 1). In the Belledonne the synclinal median has been interpreted as the trace of right-lateral strike-slip faulting in the prolongation of the Chamonix synclinorium but with very little field evidence (e.g., Gourlay, 1983; Hubard and Mancktelow, 1992). In the Aar the synclinorium has been interpreted as the root of one of the Helvetic nappes (e.g., Esher et al., 1988). Whilst alpine deformation is probably more distributed in Belledone and in Aar than in the Mont-Blanc (e.g. Choukroune and Gapais, 1983), it is very tempting to interpret these other Mesozoic synclinoriums as footwalls of steep faults similar to the MBsz. This would imply that a large breach fault with a minor dextral component affected the ECM from Aar to Belledone during the Neogene. However, this hypothesis needs to be tested by further structural and geochronologic studies.

The very high altitude of the Mont-Blanc appears to result from the interaction of two steep thrust faults, one of may still be active today (Fig. 12g). While most of the Subalpine anticlines in the hanging wall of the HBD are strongly eroded, in good agreement with the end of motion along that fault at ~15 Ma, the most external of these folds have a juvenile, whale-back morphology. This suggests either a very young age or a recent reactivation of the Bauges frontal thrust (Fig. 12g). Such observations strongly suggest that the alpine sole thrust is still active today and that shortening is still taking place N of the Penninic front. The same conclusion is reached when looking at seismologic studies (see a synthesis in chapter 5.2 of Sue and Tricart, 2003). On the other hand, south and east of the Penninic front, some structural and seismologic data suggest radial extension (e.g., Sue and Tricart, 2003), and GPS measurements tend to indicate a net extension across the Alps (Calais et al., 2002; Vigny et al., 2002). Determining the period that compression in the external part of the orogen has been coeval with extension in the internal part, and understand the mechanism for this style of deformation remains a major question for the study of continental lithosphere mechanics during collision.

Acknowlegments

We acknowledge Mr. Marc Poigniez and Mr. Vigna for helping us to access under ground samples from within the Mont-Blanc tunnel. Chamonix Mont-Blanc Helicoptères allows us to gather large samples from high altitudes. This sampling would not have been possible without the help of the PGHM, nor the kindness of the Aiguilles Rouges and StGervais natural reserves as well as the Chamonix and StGervais communes. F. Masson and the Montpellier geophysical team are thanked for their help in the field. This project was founded by a CNRS ATI grant to P.H.L. and N.A., and by the INSU / BRGM geofrance 3D program. Enthusiastic (J.M. Lardeaux) and sceptical (O. A. Pfiffner) reviews improved the final manuscript.

Appendix 1: $^{40}Ar/^{39}Ar$ techniques

High purity aliquots in the range 180-250μm were separated using heavy liquids, magnetic separation, and hand-picking. Separates were irradiated at Ford Nuclear Reactor of the University of Michigan in the L67 position for 28 hours for samples C1, C2 and C8, and 50 hours for all other samples. The J factor was estimated by analyzing duplicates of the Fish Canyon sanidine standard (28.02 My; Renne et al., 1998), irradiated between every 10 samples, yielding a 1% relative standard deviation. CaF_2 and K_2SO_4 salts were used to account for interfering nuclear reactions. Step heating analysis were performed at the $^{40}Ar/^{39}Ar$ laboratory in Clermont-Ferrand on a VG3600 mass spectrometer in a way similar to that described in Arnaud et al. (2003). Average blanks for ^{40}Ar range from 1.3x10-15 moles STP at low temperature to 4.7x10-15 moles STP at 1200°C on both furnaces and have been reproducible over the years. Blanks for other masses are usually under detection level or so low that they have large uncertainties. Age spectrum calculations are given at 1σ on each step and include all correction factors, as well as 2% errors on blanks taken for correction. Individual steps do not include error on J factor, while plateau and isochron ages do, with an average of 1.5%. Comparison of several isotopes allows qualitative analysis of K/Ca ($^{39}Ar/^{37}Ar$) and Cl/K ($^{38}Ar/^{39}Ar$) ratios. Note that for simplicity, K/Ca and Cl/K will be used in the text while no strict calculations have been made and those terms only reflect the isotope ratios. Results are shown in table 1. Plateau ages and isochrons are calculated following the criteria of Dalrymple et al. (1981) and Roddick (1980).

A particularly long furnace heating schedule was conducted on K-feldspar in order to try to retrieve diffusion characteristics, to apply diffusion models, and to calculate model thermal histories (e.g. Lovera et al., 1991).We also conducted two-stage isothermal stepwise heating at low temperatures (450-800°C); the first and the second of the two isothermal stages lasting of the order of 10 and 15 min respectively. Such a heating schedule often produces a sawtooth-shaped age spectrum where the second of the two stages is systematically younger and less affected by excess argon (e.g., Harrison et al., 1994).

We have assumed closure temperatures of 320±40°C for biotites (e.g. Harrison and Amstrong, 1978; Leloup et al, 2001). For K-feldspars, the calculation of a cooling history using diffusion models was impossible. We qualitatively considered that the lower furnace temperature (LT, 400-700°C) ages correspond to cooling at ≈150-300°C, whereas higher furnace temperatures (HT, 1000-1200°C) ages correspond to cooling at ≈300-450°C (e.g. Leloup et al, 2001).

Appendix 2: Fission-track methodology

Apatite was separated using standard magnetic and density methods, then mounted on glass slides with araldite epoxy. After grinding and polishing to expose an internal surface, the apatites were etched with 5.5 molar nitric acid for 20 seconds at 21°C. Samples were irradiated in 2 groups at Oregon State University; one of the groups had 5 times the dose of the other. After irradiation, mica external detectors were etched in 40% HF for 45 minutes at 21°C. For age determinations, 12 to 25 good-quality grains per sample were selected at random and dated using the external detector method. Laboratory procedures are essentially the same as reported in Sobel and Strecker (2003). Additional analytical details are presented in table 2. Following convention, all statistical uncertainties on pooled ages and mean track lengths are quoted at the ±1σ level, but ±2σ uncertainties are taken into account for geologic interpretation.

References

Affolter, T., Etude des deformations et restauration 3D d'un basin de front de chaîne: l'exemple du Jura et des massifs subalpins français, Joseph Fourier thesis, Joseph Fourier, Grenoble, 2003.

Affolter, T., and J.-P. Gratier, Map view retrodeformation of an arcuate fold-and-thrust belt: The Jura case, *Journal of Geophysical Research, 109*, 2004.

Antoine, P., and e. al., geological map of France (1/50 000) sheet Mont-Blanc (704), éditions du B.R.G.M., Orléans, France., 1979.

Antoine, P., J.L. Pairis, and B. Pairis, Quelques observations nouvelles sur la structure de la couverture sédimentaire interne du massif du Mont-Blanc, entre col Ferret (frontière italo-suisse) et la tête des fours (Savoie, France), *Géologie Alpine, 51*, 5– 23, 1975.

Aprahamian, J., Cartographie du métamorphisme faible à très faible dans les Alpes frabnçaises externe par l'utilisation de la cristallinité de l'illite, *Geodinamica Acta, 2*, 25-32, 1988.

Arnaud, N., P. Tapponnier, F. Roger, M. Brunel, U. Schärer, C. Wen, and Z. Xu, Evidence for Mesozoic shear along the western Kunlun and Altyn-Tagh fault, northern Tibet (China), *Journal of Geophysical Research, 108*, 2003.

Ayrton, S., Déformations des séries autochtone et Helvétique au SE du massif du Mont-Blanc, *Eclogae Geologicae Helveticae, 62*, 95-104, 1969.

Ayrton, S., La géologie de la zone Martigny-Chamonix (versant Suisse) et l'origine de la nappe de Morcles (un exemple de subduction continentale)*, 73*, 137-172, 1980.

Baggio, P., Contributo alla conoscenza geologica del versante italiano del Monte Bianco, *Atti Ist. Veneto Sci., 122*, 293-325, 1964.

Baggio, P., G. Ferrara, and R. Malaroda, results of some Rb/Sr age determinations of the rocks of the Mont Blanc tunnel, *Bolletin della societa geologica Italiana, 86*, 193-212, 1967.

Beck, C., E. Deville, E. Blanc, Y. Philippe, and M. Tardy, Horizontal shortening control of the Middle Miocene marine siliciclastic accumulation (Upper Marine Molasse) in the southern termination of the Savoy Molasse Bassin (northwestern Alps / southern Jura), in *Cenozoic foreland basins of western Europe*, vol. 134, *Geological society Special Publications*, edited by M. Fernandez, pp. 263-278, 1998.

Becker, A., The Jura mountains: an active foreland fold-and-thrust belt?, *Tectonophysics, 321*, 381-406, 2000.

Bellière, J., Caractère de la déformation Alpine dans les schistes cristallins du massif du Mont-Blanc, *Bulletin de la Société Geologique de France, VI*, 691-698, 1956.

Bellière, J., On the age of mylonites within the Mont-Blanc massif, *Geodinamica Acta, 2*, 13-16, 1988.

Bellière, J., and e. al., geological map of France (1/50 000) sheet Chamonix (680), éditions du B.R.G.M., Orléans, France, 1987.

Bertini, G., M. Marcucci, R. Nevini, P. Passerini, and G. Sguazzoni, Patterns of faulting in the Mt Blanc granite, *Tectonophysics, 11*, 65-106, 1985.

Bonin, B., P. Brändlein, F. Bussy, J. Desmons, U. Eggenberger, F. Finger, K. Graf, C. Marro, I. Mercolli, R. Oberhänsli, A. Ploquin, A. Von Quadt, J. Von Raumer, U. Schaltegger, H.P. Steyrer, D. Vison, and G. Vivier, Late Variscan magmatic evolution of the alpine basement, in *Pre-Mesozoic geology in the Alps*, edited by J.V. Raumer and Neubauer, Springer-Verlag, Berlin Heidelberg, New York, 1993.

Bussy, F., Pétrogénèse des enclaves microgrenues associées aux granitoïdes calc-alcalins: example des massifs varisque du Mt-Blanc (Alpes occidentales) et Miocène du Monte Capanne (Ile d'Elbe, Italie), Ph.D thesis, Lausanne (switzerland), 1990.

Bussy, F., J. Hernandez, and J.V. Raumer, Bimodal magmatism as a consequence of the post-collisional readjustment of the thickened Variscan continental lithosphere (Aiguilles Rouges-Mont-Blanc massifs, western Alps), *Special paper of the Geological Society of America, 350*, 221-233, 2001.

Bussy, F., and J.V. Raumer, U-Pb dating of Palaezoic events in the Mont-Blanc crystalline massif, Western Alps, in *European union of geosciences*, vol. Terra abstracts, abstract suplement n°1 to Terra Nova n°5, pp. 382, Strasbourg, France, 1993.

Bussy, F., U. Schaeltegger, and C. Marro, The age of the Mont-Blanc granite (western Alps): a heterogeneous isotopic system dated by Rb-Sr whole rock determinations on its microgranular enclacves, *Scweizerishe Mineralogische und petrographische Mitteilungen, 69*, 3-13, 1989.

Butler, R., Balanced cross-sections and their implications for deep structure of the northwest Alps,, *Journal of Structural Geology, 5*, 125-138, 1983.

Butler, R., The restoration of thrust systems and displacement continuity around the Mont-Blanc massif, NW external Alpine thrust belt, *Journal of Structural Geology, 7*, 569-582, 1985.

Calais, E., J.M. Nocquet, F. Jouanne, and M. Tardy, Current strain regime in the western Alps from continuous Global Positioning System measurements 1996-2001, *Geology, 30*, 651-654, 2002.

Capuzzo, N., and F. Bussy, Volcanic input in a late Paleozoic tectono-sedimentary basin: the Salvan-Dorénaz basin (South-westen Switzerland – Eastern France), in *EUG 10*, vol. 11, *Terra Abstracts*, pp. 297, Strasbourg, France, 1999.

Capuzzo, N., R. Handler, F. Neubauer, and A. Wetzel, Post-collisional rapid exhumation and erosion during continental sedimentation: the example of the late Variscan Salvan-Dorénaz basin (Western Alps), *International Journal of Earth Sciences, 92*, 364-379, 2003.

Carpéna, J., Fission-track dating of zircons: zircons from Mont Blanc granite (French-Italian Alps), *Journal of geology, 100*, 411-421, 1992.

Choukroune, P., and D. Gapais, strain pattern in the Aar granite (central Alps) : orthogneiss developed by bulk inhomogeneous flattening, *Journal of Structural Geology, 5*, 1-10, 1983.

Crespo-Blanc, A., H. Masson, Z. Sharp, M. Cosca, and J. Hunziker, A stable and $^{40}Ar/^{39}Ar$ isotope study of a major thrust in the Helvetic nappes (Swiss Alps): evidence for fluid flow and constraints on the nappe kinematics, *Geological Society of America Bulletin, 107*, 1129-1144, 1995.

Dalrymple, G.B., E.C. Alexander, Jr., M.A. Lanphere, and G.P. Kraker, *Irradiation of samples for $^{40}Ar/^{39}Ar$ dating using the Geological Survey TRIGA reactor*, 55 pp., U. S. Geological Survey, Reston, VA, 1981.

Deville, E., Blanc, E. , M. Tardy, C. Beck, M. Cousin, and G. Ménard, Thrust propagation and syntectonic sedimentation in the Savoy Tertiary Molasse Basin (Alpine foreland), in *Hydrocarbon and petroleum geology of France*, vol. 4, *E.A.P.G. Spec. Publ.*, edited by A. Mascle, pp. 269-280, 1994.

Eltchaninoff-Lancelot, C., S. Triboulet, B. Doudoux, S. Fudral, J.P. Rampnoux, and M. Tardy, Stratigraphie et tectonique des unités delphino-helvétiques comprises entre Mont-Blanc et Belledone (Savoie – Alpes occidentales). Implications régionales, *Bulletin de la Société Geologique de France, XXIV*, 817-830, 1982.

Epard, J.L., Le contact entre le socle du Mont-Blanc et la zone de Chamonix: implications tectoniques, *Bulletin de la société Vaudoise de sciences naturelles, 78*, 225-245, 1986.

Epard, J.L., *La nappe de Morcles au Sud-Ouest du Mont-Blanc*, Lausanne, 1990.

Escher, A., H. Masson, and A. Steck, Coupes géologiques des Alpes occidentales suisses, Service hydrologique et géologique national, Berne (Switzerland), 1988.

Escher, A., H. Masson, and A. Steck, Nappe geometry in the western Swiss Alps, *Journal of Structural Geology, 15*, 501-509, 1993.

Fabre, C., M.C. Boiron, J. Dubessy, M. Cathelineau, and D.A. Banks, Palaeofluid chemistry of a single fluid event: a bulk and in-situ multi-technique analysis (LIBS, Raman spectroscopy) of an Alpine fluid (Mont-Blanc), *Chemical geology, 182*, 249-264, 2002.

Fügenschuh, B., and S.M. Schmid, Late stages of deformation and exhumation of an orogen constrained by fission-track data: a case study in the western Alps, *G.S.A. Bulletin, 115*, 1425-1440, 2003.

Gidon, M., Les massifs cristallins externes des Alpes occidentals françaises sont-ils charriés?, *Géologie Alpine, 77*, 23-38, 2001.

Gourlay, P., Le jeu décrochant dextre tardif de la suture de Chamonix (Alpes françaises et suisses), *Comptes Rendus à l'Académie des Sciences de Paris, 296, série 2,*, 927-932, 1983.

Gourlay, P., La déformation du socle et des couvertures delphino-helvétiques dans la région du Mont-Blanc (Alpes occidentales), *Bulletin de la Société Geologique de France, (8) II*, 159-169, 1986

Grasmück, K., Die helvetishen Sedimente am Nordostrand des Mont-Blanc-Massivs (zwishen Sembrancher und dem Col Ferret), *Eclogae Geologicae Helveticae, 54*, 351-450, 1961.

Green, P.F., I.R. Duddy, A.J.W. Gleadow, and J.F. Lovering, Apatite fission-track analysis as a paleotemperature indicator for hydrocarbon exploration, in *Thermal History of Sedimentary Basins: Methods and Case Histories*, edited by a.T.H.M. in N. D. Naeser, pp. 181-195, Springer-Verlag, New York, 1989a.

Green, P.F., I.R. Duddy, G.M. Laslett, K.A. Hegarty, A.J.W. Gleadow, and J.F. Lovering, Thermal annealing of fission-tracks in apatite, 4, Quantitative modelling techniques and extension to geological timescales, *Chemical geology, 79*, 155-182, 1989b.

Guellec, S., J.-L. Mugnier, M. Tardy, and F. Roure, Neogene evolution of the western Alpine foreland in the light of ECORS data and balanced cross-section, in *deep structure of the Alps*, *Mem. Soc. Geol. France*, edited by R. Polino, pp. 165-184, 1990.

Guermani, A., and G. Pennacchioni, Brittle precursors of plastic deformation in a granite: an exemple from the Mont-Blanc massif (Helvetic, western Alps), *Journal of Structural Geology, 20*, 135 – 148, 1998.

Harrison, T.M., R.L. Amstrong, and G.K.C. Clarke, Thermal models and cooling histories from fission-track, K-Ar, Rb-Sr and U-Pb mineral dates, northern coast plutonic complex, British Columbia., in *fourth international conference, geochronology, cosmochronology, isotope geology*, edited by Z.R.E.e. U. S. geological survey, pp. 167-170, 1978.

Harrison, T.M., M.T. Heizler, O.M. Lovera, Chen Wenji, and M. Grove, A chlorine disinfectant for excess argon released from K-feldspar during step heating, *Earth & Planetary Science Letter, 123*, 95-104, 1994.

Hubbard, M., and N.S. Mancktelow, Lateral displacement during Neogene convergence in the western and central Alps, *Geology, 20*, 943-946, 1992.

Huon, S., M. Burkhard, and J.C. Hunziker, Mineralogical, K/Ar, stable and Sr isotope systematics of K-white micas during very low grade metamorphism of limestones (Helvetic nappes, western Switzerland), *Chemical geology, 113*, 347-376, 1994.

Hurford, A.J., Cooling and uplift patterns in the Lepontine Alps South Central Switzerland and age of vertical movement on the Insubric fault line, *Contributions to Mineralogy and Petrology, 92*, 423-427, 1986.

Jan du Chêne, R., Etude palynologique du Néogène et du Pléistocène inférieur de Bresse (France), PhD thesis, Université de Genève, Genève, 1974.

Ketcham, R.A., R.A. Donelick$, and W.D. Carlson, Variability of apatite fission-track annealing kinetics: III. Extrapolation to geological time scales, *American mineralogist, 84*, 1235-1255, 1999.

Kirschner, D.L., Z.D. Sharp, and H. Masson, Oxygen isotope thermometry of quartz-calcite veins : unraveling the thermal-tectonic history of the subgreenschist facies Morcles nappe(Swiss Alps), *Geological Society of America Bulletin, 107*, 1145-1156, 1995.

Kirschner, L., M.A. Cosca, H. Masson, and J.C. Hunziker, Staircase 40Ar/39Ar spectra of fine-grained white mica: timing and duration of deformation and empirical constraints on argon diffusion, *Geology, 24*, 747-750, 1996.

Lacassin, R., P. Tapponnier, and L. Bourjot, Culminations d'échelle crustale et imbrication de la lithosphère dans les Alpes, apports du profil ECORS-CROP, *Comptes Rendus à l'Académie des Sciences de Paris, 310, série II*, 807-814, 1990.

Leloup, P.H., N. Arnaud, R. Lacassin, J.R. Kienast, T.M. Harrison, P.T. Trinh, A. Replumaz, and P. Tapponnier, New constraints on the structure, thermochronology and timing of the Ailao Shan - Red River shear zone, SE Asia., *Journal of Geophysical Research, 106*, 6683-6732, 2001.

Lemoine, M., P.C.d. Graciansky, and P. Tricart, *De l'océan à la chaîne de montagnes – Tectonique des Plaques des Alpes*, 207 pp., Gordon and Breach Science Publishers, 2000.

Leutwein, F., B. Poty, J. Sonet, and J.-L. Zimmermann, Age des cavités à cristaux du granite du Mont-Blanc, *Comptes Rendus à l'Académie des Sciences de Paris, t. 271, série D*, 1970.

Lovera, O.M., F.M. Richter, and T.M. Harrison, Diffusion domains determined by 39Ar released during step heating, *Journal of Geophysical Research, 96*, 2057-2069, 1991.

Marshall, D., D. Kirschner, and F. Bussy, A variscan pressure-temperature-time-path for the N-E Mont-Blanc massif, *Contributions to Mineralogy and Petrology, 126*, 416-428, 1997.

Marshall, D., N. Meisser, and R.P. Taylor, Fluid inclusion, stable isotope and Ar-Ar evidence for the age and origin of gold-bearing quartz veins at Mont Chemin, Switzerland, *Mineralogy and Petrology, 62*, 147-165, 1998a.

Marshall, D., H.R. Pfeifer, J.C. Hunziker, and D. Kirschner, A pressure-temperature-time path for the NE Mont-Blanc massif: fluid-inclusion, isotopic and thermobarometric evidence, *European journal of mineralogy, 10*, 1227-1240, 1998b.

Masson, F., F. Gal, and P.H. Leloup, Une carte gravimétrique haute résolution du massif du Mont-Blanc: implications structurales, *Comptes rendus Geosciences, 334*, 1011-1019, 2002.

Masson, H., Un siècle de géologie des Préalpes: de la découverte des nappes à la recherche de leur dynamique, *Eclogae Geol. Helv., 73*, 331-349, 1976.

Mattauer, M., Les subductions intracontinentales des chaînes tertiaires d'Asie; leurs relations avec les décrochements, *Bulletin de la Société Géologique de France, 8*, 143-157, 1986.

Ménard, G., and T. F., Coupes equilibrees crustales; methodologie et application aux Alpes occidentales, *Geodinamica Acta, 1*, 35-45, 1987.

Mennessier, G., F. Carme, J. Bellière, R. Dhellemes, P. Antoine, and N. Oulianoff, geological map of France (1/50 000) sheet St Gervais-les-Bains (703), éditions du B.R.G.M., Orléans, France, 1976.

Nicolas, A., R. Polino, A. Hirn, R. Nicolich, and ECORS-CROP working group, ECORS-CROP traverse and deep structure of the western Alps. A synthesis., in *Deep structure of the Alps*, vol. 156, *Mém. Soc. Geol. Fr.*, edited by R. Polino, pp. 15-27, Paris, 1990.

Pairis, J.L., and e. al., geological map of France (1/50 000) sheet Cluses (679), éditions du B.R.G.M., Orléans, France, 1993.

Pfiffner, O.A., The structure of the Helvetic nappes and its relation to the mechanical stratigraphy, *Journal of Structural Geology, 15*, 511-521, 1993.

Pfiffner, O.A., P. Lehner, P. Heitzmannet, M. S., and S. A., Deep structure of the Swiss Alps: Results of NRP 20, Birkhäuser, Boston Cambridge, Mass., 1997.

Pfiffner, O.A., F. Schlunegger, and S.J.H. Buiter, The Swiss Alps and their peripheral foreland bassin : stratigraphic response to deep crustal processes, *Tectonics, 21*, 3-1 to 3-16, 2002.

Platt, J.P., Balanced cross-sections and their implications for the deep structure of the northwest Alps : discussion, *Journal of Structural Geology, 6*, 5, 1984.

Poty, B., and M. Cathelineau, La formation des cristaux dans les fentes alpines du massif du Mont-Blanc, *le règne minéral, hors série n°V*, 19-21, 1999.

Poty, B., H.A. Stalder, and A.M. Weisbrod, Fluid inclusions studies in quartz from fissures of western and central Alps, *Schweizerishe Mineralogische und petrographische Mitteilungen, 54*, 717-752, 1974.

Ramsay, J.G., Tectonics of the Helvetic nappes, in *Thrust and nappe tectonics*, vol. 9, *special publication of the geological society of london*, edited by K.R.M.a.N.J. Price, pp. 293-309, 1981.

Renne, P.R., C.C. Swisher, A.L. Deino, D.B. Karner., T.L. Owens, and D.J. DePaolo, Intercalibration of standards, absolute ages and uncertainties in 40Ar/ 39Ar dating, *Chemical geology, 145*, 117-152, 1998.

Roddick, J.C., R.A. Cliff, and D.C. Rex, The evolution of excess argon in alpine biotites, a 40Ar/39Ar analysis, *Earth & Planetary Science Letter, 48*, 185-208, 1980.

Rolland, Y., S. Cox, A.-M. Boullier, G. Pennacchioni, and N. Mancktelow, Rare earth and trace element mobility in mid-crustal shear zones: insights from the Mont Blanc Massif (Western Alps), *Earth & Planetary Science Letter, 214*, 203-219, 2003.

Rossi, M., Y. Rolland, O. Vidal, and S.F. Cox, Geochemical variations and element transfer during shear zone development and related episyenites at middle crust depths: insights from the Mont-Blanc granite (French-Italian Alps). in *High strain zones: structure and physical properties*, *Geol. Soc. London special publication*, edited by D. Brunh and L. Burlini, in press.

Ruffini, R., M. Cosca, A. d'Atri, J. C. Hunziker, and R. Polino, The volcanic supply of the Taveyanne turbidites (Savoie, France) : A riddle for Tertiary Alpine volcanism, *Atti delle Accademia Scienze Roma, 14*, 359-376, 1995.

Schmid, S.M., and E. Kissling, The arc of the western Alps in the light of geophysical data on deep crustal structure, *Tectonics, 19*, 62-85, 2000.

Seward, D., and N.S. Mancktelow, Neogene kinematics of the central and western Alps : evidence from fission-track dating, *Geology, 22*, 803-806, 1994.

Sobel, E.R., and M.R. Strecker, Uplift, exhumation, and precipitation: Tectonic and climatic control of Late Cenozoic landscape evolution in the northern Sierras Pampeanas, Argentina, *Basin Research, 15*, 2003.

Soom, M.A., Abkühlungs- und Hebungsgeschichte der Externmassive und der Penninischen decken beidseits der Simplon-Rhone-Linie seit dem Oligozän : Spaltspurdatierungen an apatit/zirkon und K/Ar-datierungen an biotit/muskowit (westliche zentralalpen), Ph. D thesis, 119 pp., University of Bern, Bern (switzerland), 1990.

Sue, C., and P. Tricart, Neogene to ongoing normal faulting in the inner western Alps: a major evolution of the late alpine tectonics, *Tectonics, 22*, 1050, 2003.

Thouvenot, F., J. Fréchet, L. Jenatton, and J.-F. Gamond, The Belledonne border fault: identification of an active seismic strike-slip fault in the western Alps, 2003.

Vigny, C., and and al., GPS network monitors the western Alps over a five year period: 1993-1998, *Journal of geodesy, 76*, 63-76, 2002.

Von Raumer, J.F., Zur Metamorphose amphibolitisher Gesteine im Altkristallin des Mont-Blanc und Aiguilles Rouges Massivs, *Schweizerische mineralogishe und petrographiche Mitteilungen, 54*, 471-488, 1967.

Von Raumer, J.F., Kristallization und gefügebildung im Mont-Blanc granit, *Schweizerishe Mineralogische und petrographische Mitteilungen, 47*, 499-579, 1974.

Von Raumer, J.F., J. Abrecht, F. Bussy, B. Lombardo, M. R.P., and U. Schaltegger, The Palaeozoic evolution of the external massifs, *Schweizerishe Mineralogische und petrographische Mitteilungen, 79*, 5-22, 1999.

Von Raumer, J.F., and Neubauer, Pre-Mesozoic geology in the Alps, Springer-Verlag, Berlin Heidelberg, New York, 1993.

Figures caption

Fig. 1 Structural framework of the western Alps

Common legend for a) and b). **a)** Structural map of the western Alps. **b)** large-scale geological cross-section of the western Alps. Modified from Lacassin et al (1990).

Fig. 2 Structure of the Mont-Blanc massif.

a) Structural map of the Mont-Blanc massif. The map is drawn from published geological maps: Mont-Blanc (Antoine et al., 1979); Chamonix (Bellière et al.; 1987); Cluses (Pairis et al.; 1993) and St Gervais-les-Bains (Mennessier et al., 1976), as well as personal observations. **b)** Synthetic cross-section of the Mont-Blanc massif. Based on our observations (see also Fig. 5). HBD is the Helvetic basal décollement. Note that this section is compatible with recent gravity data of the area (Masson et al., 2002). See section 3.6 of the text for discussion on the relative timing of deformation events.

Fig. 3 Deformation in the Mont-Blanc massif

For pictures locations see Fig. 2a. **a)** High glaciated peaks of the Mont-Blanc massif viewed from the WNW. View from Cordon above Sallanches. This landscape is an oblique view of the central part of the section shown in Fig. 2b. **b)** Aplitic veins intruding the Variscan gneisses. SW part of the Mont-Blanc massif above the Nid D'aigle. **c)** Schistosity and stretching lineation in Liassic shales in Combes des fonds of the Swiss Val Ferret, corresponding to the root of the Helvetic nappes. Li indicates the lineation direction (see Fig. 4a). Hammer gives scale. **d)** Sheared calcite veins in Liassic shales of the Swiss Val Ferret indicating top to the NW thrusting. Compass gives scale. **e)** Back-thrusting of the Mont-Blanc granite on top of the steepened Liassic series of the Italian Val Ferret. Picture from the pathway to the Bocallette refuge, S of the Grandes Jorasses. The inset is the corresponding cross-section. **f)** Thin section of Mesozoic calcschists of the Chamonix syncline. Vormaine ridge, near Le Tour (see Fig. 5c). The rock shows a strong schistosity (21E57) and lineation (pitch72N), (Fig. 4c). The shear planes (C) indicate a top to the NW sense of shear parallel to motion in Mont-Blanc shear zone (Fig. 4c & d). **g)** Alpine stretching lineation in othogneissess (Ordovician protolith) E of Argentière. Foliation N15 67E, lineation pitch 77N (see Fig. 4d). **h)** Sheared aplitic vein in the Argentière orthogneisses. The inset shows S/C structures in orthogneiss. C planes shallower than the foliation indicate thrusting to the NW. **i)** Polished slab of sample ME 137 from an alpine shear zone affecting the Variscan gneiss. Foliation N60 48S, lineation pitch 75E. S/C relationships indicate thrusting to the NW. **j)** Thin section of sample ME37. Echelles du Montenvers. Foliation N20 65S, lineation pitch 90. S/C relationships indicate thrusting to the NW.

<u>Fig. 4</u> Structural data of the Mont-Blanc massif.

Schmidt lower hemisphere projection. **a)** Schistosities and stretching lineations from the root zone of the Helvetic nappes. Measurements along the Swiss Val Ferret, within Mesozoic sediments (white symbols) and the Mont Blanc granite (black symbols). The average schistosity pole trends N292 25° (39 data, K=26.2), corresponding to an average plane trending N22 65 E. The average lineation trends N134 64° (35 data, K=17.5). The black dotted lines refer to the range of data observed in the Chamonix synclinorium (see Fig. 4c). **b)** Variscan foliations. Foliations ascribed to Variscan deformations *s.l.* (see text for details). These data includes foliations of Paleozoic rocks within the Posette synclinorium (white symbols); (Fig.5c). The average foliation pole trends N288 25° (48 data, K=6.5), corresponding to an average plane trending N48 65 E. Note that their are only a few lineations, most of them dipping shallowly. **c)** Schistosities and lineations within the Mezosoic sediments of the Chamonix synclinorium. The two lineation and foliation groups are ascribed to two distinct structures: the tilted décollement at the base of the Helvetic nappes (dotted lines) and the Mont-Blanc shear zone (long dashed lines). Black symbols refer to shear planes affecting the Aiguilles Rouges basement. See text for details. **d)** Mont-Blanc shear zone. Foliations ascribed to Alpine deformations within the Mont Blanc shear zone (see text for details). Data include medium temperature lineation from the NW flank of the Mont-Blanc (black symbols) as well as low temperature lineations mostly from the Nid d'Aigle area (white symbols). The average foliation pole trends N306 42° (108 data, K=15.5), corresponding to an average plane trending N36 48 E. The black long dashed lines refer to the range of data observed in the Chamonix synclinorium (see Fig. 4c)

<u>Fig. 5</u> Cross sections of the NW flank of the Mont-Blanc massif.

NW-SE cross sections from the northern to the southern extremity of the massif (sections 1 to 8, respectively). See Figure 2a for locations. No vertical exaggeration.

Fig. 6 Brittle faults of NW flank (Nid d'Aigle) and SE flank of the Mont-Blanc massif.

Brittle faults from the Nid d'Aigle area are shown in gray while those from the SE flank of the massif are in black. Arrows mark the direction of motion of the upper block when it could be confidently determined. The Mont-Blanc shear zone is shown in light gray for comparison. The thick dashed planes correspond to the contact between the granite and the sedimentary series along the Mont-Blanc back-thrust, below the Boccalatte refuge (B), near Pra Sec (Pr) and at Peuterey (P). The dextral strike-slip faults correspond to re-activated schistosity planes within Mesozoic sediments of the Val Ferret and Val Veni. The faults likely correspond to two and maybe three direction of the maximum horizontal stress (σhmax), (see text for details). Schmidt lower hemisphere projection.

<u>Fig. 7</u> Alpine P-T estimates in the Mont-Blanc massif.

1 to 9: P-T estimates from fluid inclusions in alpine veins. 1: Poty et al., 1974; 2 (early H20-NaCl rich fluids) and 3 (late H20-CO2 fluids): Poty and Cathelineau, 1999; 4 (Helbronner): Fabre et al., 2002; 5: (Qtz-Chl veins), 7 (Qtz-Mu veins), 8 (Stilp-Epi-Cc-Qtz veins) and, 9 (Par-Kat. Schist) all in the NE part of Mont-Blanc: Marshall et al., 1998b, 6 (Qtz-gold veins, in the NE part of Mt-Blanc): Marshall et al., 1998a; 10 musc-chlorite equilibria in a musc-biot-chl mylonite within the granite (Rolland et al., 2003). References: [1] Marshall et al., 1998b; [2] Marshall et al., 1998a; [3] Kirschner et al., 1995. Nappe thicknesses have been measured from classical cross-sections (e.g. Escher et al., 1988). The data appear to describe the alpine P-T path of the Mont-Blanc. Bold ages denote first order time milestones deduced from geochronological data; see text for discussion.

Fig. 8 Timing constrains on the main Alpine deformations within the Mont-Blanc and Aiguilles Rouges massifs.

References are: [1] Huon et al., 1994; [2] Ruffini et al., 1995; [3] Kirschner, 1996; [4] Crespo-Blanc et al., 1995; [5] Marshall et al., 1998a; [6] Leutwein et al., 1970; [7] Krummenacher and Evernden, 1960; [8] this study; [9] Baggio et al., 1967; [10] Marshall et al., 1998b; [11] Soom, 1990.; [12] Seward and Mancktelow, 1994; [13] Carpéna 1992; [14] Pfiffner et al., 2002; [15] Beck et al., 1998 and Deville et al., 1994; [16] Becker, 2000; [17] Jan du Chêne, 1974. The light gray area encompasses the timing of uplift of the Aiguilles Rouges and Mont-Blanc massif.

Fig. 9 Location of new $^{40}Ar/^{39}Ar$ and fission-track data.

Location of samples analysed for fission-track and $^{40}Ar/^{39}Ar$ thermochronology. The figure frame is located on Fig. 2a.

Fig. 10 Examples of new $^{40}Ar/^{39}Ar$ data.

a) Biotite age spectra of samples C2, C1 and ME25. **b)** Biotite age spectra of samples C8, and ME50. **c), e), g)** Kf ages spectra for samples ME41, C2 and ME27. **d), f), h)** $^{38}Ar/^{39}Ar$ (proxy for the Cl/K) and $^{39}Ar/^{37}Ar$ (proxy for the K/Ca) spectra respectively of samples ME41, C2 and ME27.

Fig. 11 New fission-track results.

a) Plot of apatite fission-track ages versus altitude. **a1**: all ages. a2: ages from the Mont-Blanc massif along section 6. a3: ages from the Belledonne massif. a4: ages from the Aiguilles Rouges massif. [12] from Seward and Mancktelow, (1994). RS 4 comes from the NE Mont-Blanc near Martigny. For other samples locations see Fig. 9. **b)** Cross section of the Mont-Blanc massif at the level of the tunnel (6 on Fig. 9a) with apatite FT sample numbers and ages (see Table 2).

Fig. 12 Structural evolution of the external Alps.

a-g) Structural evolution of the external Alps along a NW-SE section across the Aiguilles Rouges and Mont-Blanc massifs, depicted seven time steps from 50 Ma ago to present day. Note that the structural evolution of the internal Alps, mostly occurring before 32 Ma, is not depicted. Shortening estimates in the Jura and Helvetic nappes from Affolter (2003). A to D refer to the main deformation phases in the Aiguilles Rouges and Mont-Blanc massifs (see also Fig. 2b and Fig. 8). Note that the bottom line of the section does not corresponds to the Moho but rather to a passive marker at the top of the layered lower crust **h)** ECORS-CROP seismic line for broad comparison with g). From Schmid and Kissling (2000). Some structures, such as the Mont-Blanc back-thrust, are offset from this seismic line, which goes through Belledonne south of the Mont-Blanc (see Fig. 1a).

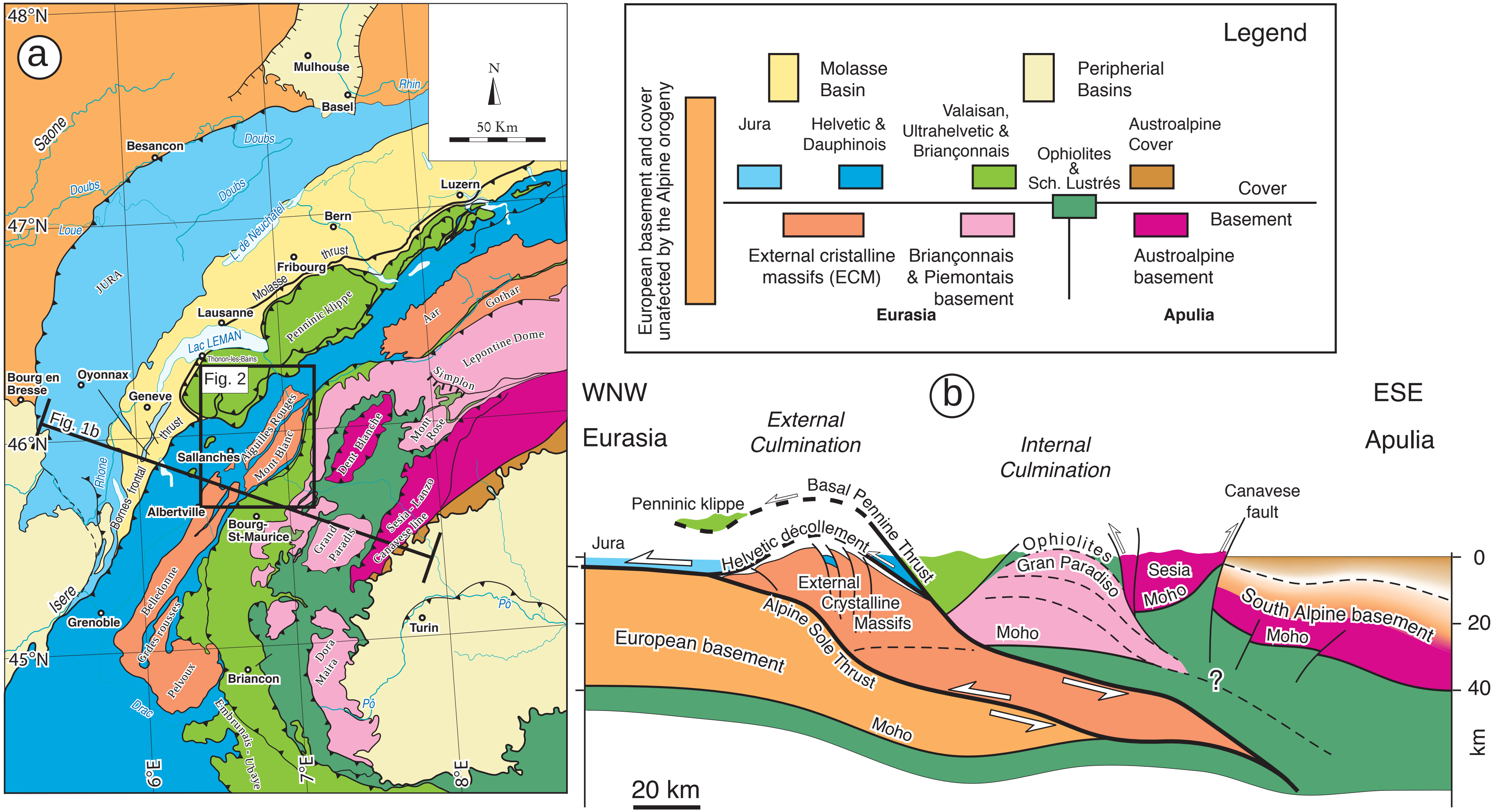
a
48°N
47°N
46°N
45°N
6°E
7°E
8°E
N
50 Km
Mulhouse
Basel
Rhin
Saone
Besancon
Doubs
Luzern
Bern
Fribourg
thrust
Loue
JURA
L. de Neuchâtel
Molasse
Lausanne
Penninic klippe
Aar
Gothar
Leponrine Dome
Simplon
Lac LEMAN
Thonon-les-Bains
Fig. 2
Bourg en Bresse
Oyonnax
Geneve
Fig. 1b
thrust
Rhone
Sallanches
Aiguilles Rouges
Mont Blanc
Dent Blanche
Mont Rose
Bornes
frontal
Albertville
Bourg-St-Maurice
Grand Paradis
Sesia - Lanzo
Canavese line
Isere
Belledonne
Grandes rousses
Grenoble
Pelvoux
Drac
Briancon
Embrunais - Ubaye
Dora Maira
Pô
Turin
Legend
Molasse Basin
Peripherial Basins
European basement and cover unafected by the Alpine orogeny
Jura
Helvetic & Dauphinois
Valaisan, Ultrahelvetic & Briançonnais
Ophiolites & Sch. Lustrés
Austroalpine Cover
Cover
Basement
External cristalline massifs (ECM)
Briançonnais & Piemontais basement
Austroalpine basement
Eurasia
Apulia
b
WNW
Eurasia
ESE
Apulia
External Culmination
Internal Culmination
Penninic klippe
Basal Pennine Thrust
Jura
Helvetic décollement
Ophiolites
Gran Paradiso
Canavese fault
Sesia
Moho
External Crystalline Massifs
Alpine Sole Thrust
European basement
Moho
South Alpine basement
?
0
20
40
km
20 km

Fig. 1

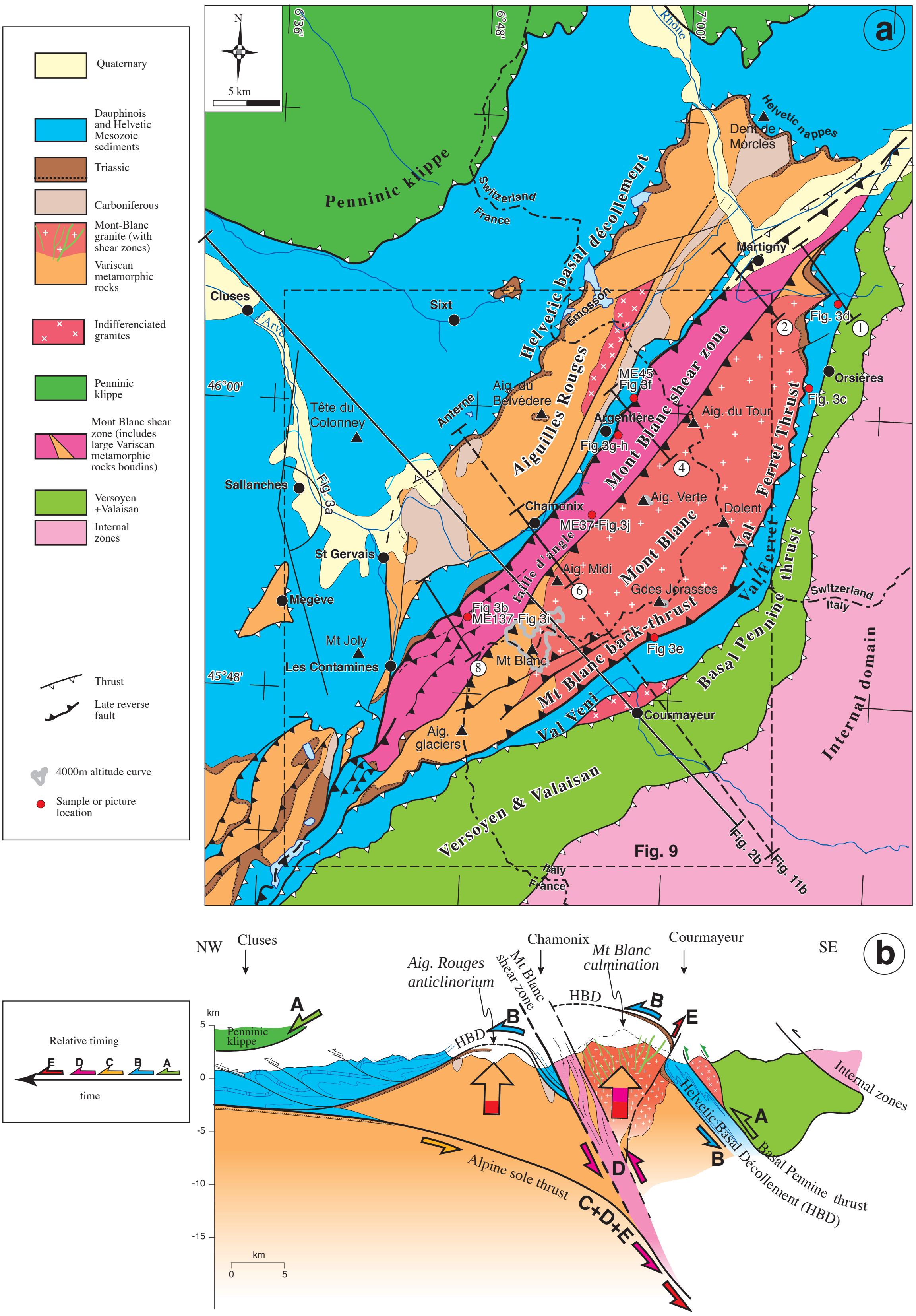
Quaternary
Dauphinois and Helvetic Mesozoic sediments
Triassic
Carboniferous
Mont-Blanc granite (with shear zones)
Variscan metamorphic rocks
Indifferenciated granites
Penninic klippe
Mont Blanc shear zone (includes large Variscan metamorphic rocks boudins)
Versoyen +Valaisan
Internal zones
Thrust
Late reverse fault
4000m altitude curve
Sample or picture location
a
Penninic klippe
Helvetic basal décollement
Aiguilles Rouges
Mont Blanc shear zone
Mont Blanc
Val Ferret Thrust
Basal Pennine thrust
Mont Blanc back-thrust
Val Veni
Versoyen & Valaisan
Internal domain
Helvetic nappes
Cluses
Sixt
Sallanches
St Gervais
Megève
Les Contamines
Chamonix
Argentière
Martigny
Orsières
Courmayeur
Fig. 9
Fig. 2b
Fig. 11b
b
Relative timing
time
NW
SE
Cluses
Chamonix
Courmayeur
Aig. Rouges anticlinorium
Mt Blanc culmination
Mt Blanc shear zone
HBD
Penninic klippe
Alpine sole thrust
C+D+E
Helvetic Basal Décollement (HBD)
Basal Pennine thrust
Internal zones

Fig. 2

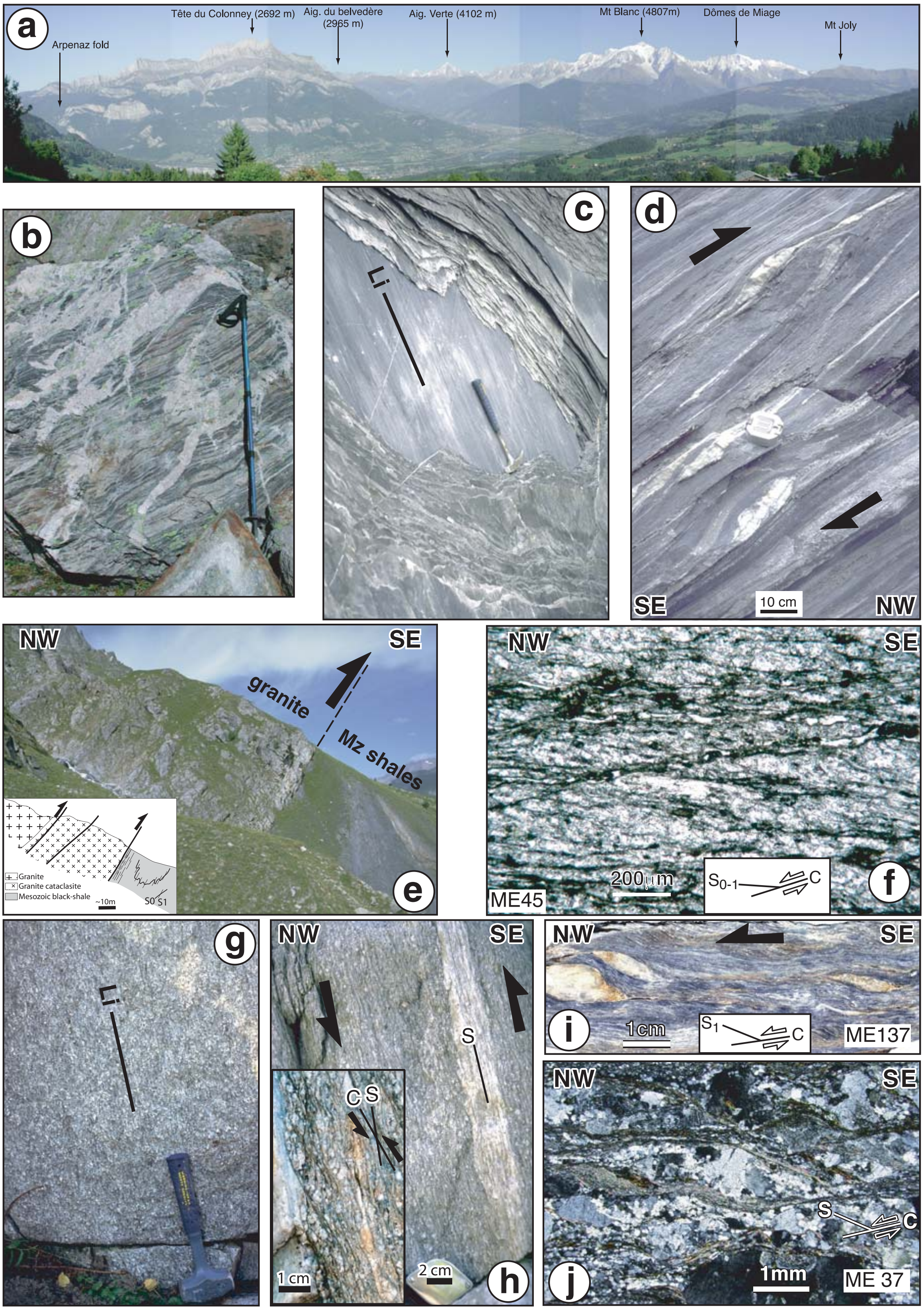
a
Arpenaz fold
Tête du Colonney (2692 m)
Aig. du belvedère (2965 m)
Aig. Verte (4102 m)
Mt Blanc (4807m)
Dômes de Miage
Mt Joly
b
c
Li
d
SE
10 cm
NW
e
NW
SE
granite
Mz shales
Granite
Granite cataclasite
Mesozoic black-shale
~10m
S0 S1
f
NW
SE
200 μm
ME45
S0-1
C
g
Li
h
NW
SE
S
C S
1 cm
2 cm
i
NW
SE
1cm
S1
C
ME137
j
NW
SE
S
C
1mm
ME 37

Fig. 3

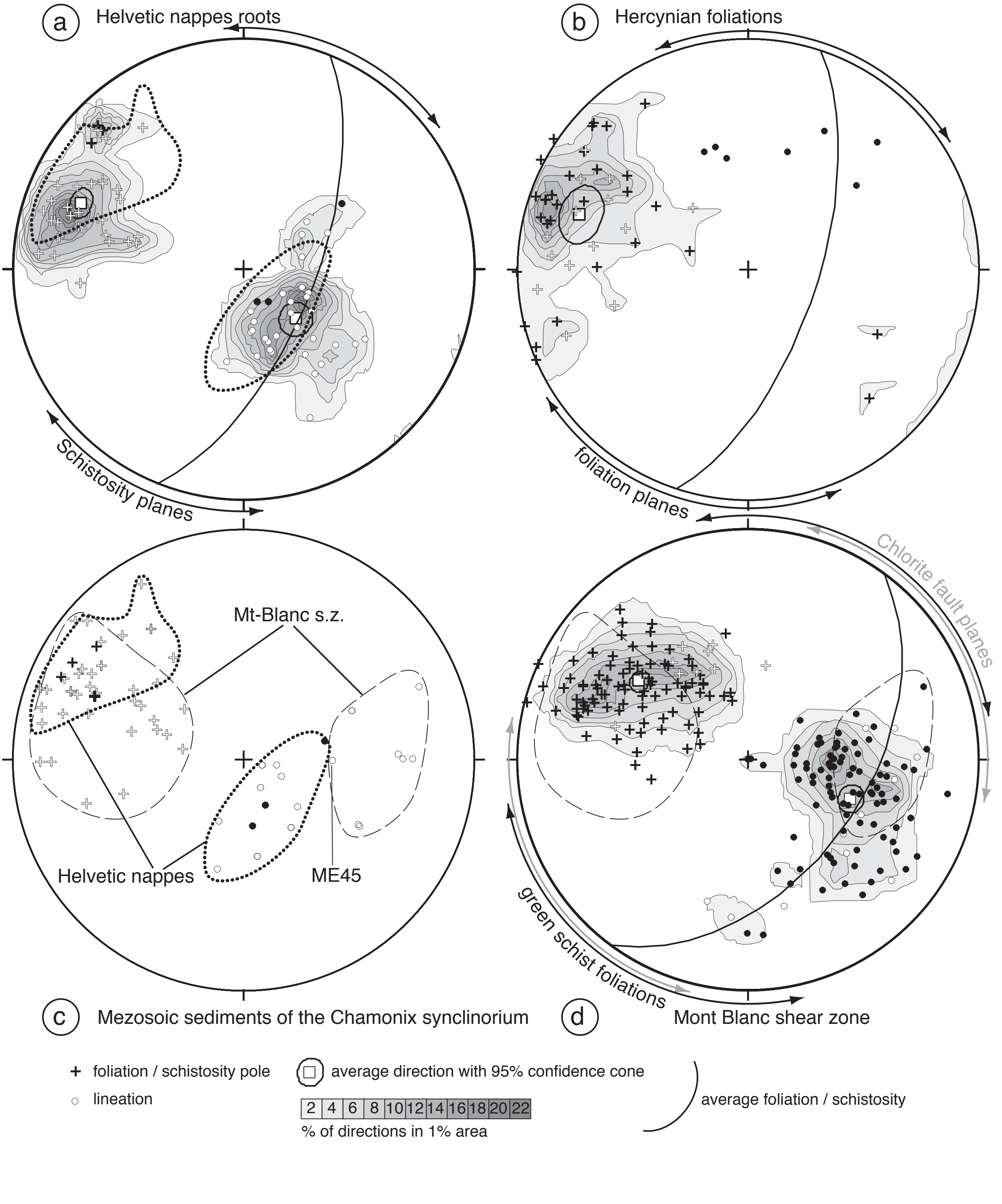

a Helvetic nappes roots
Schistosity planes
b Hercynian foliations
foliation planes
Mt-Blanc s.z.
Helvetic nappes
ME45
Chlorite fault planes
green schist foliations
c Mezosoic sediments of the Chamonix synclinorium
d Mont Blanc shear zone
foliation / schistosity pole
lineation
average direction with 95% confidence cone
2 4 6 8 10 12 14 16 18 20 22
% of directions in 1% area
average foliation / schistosity

Fig. 4

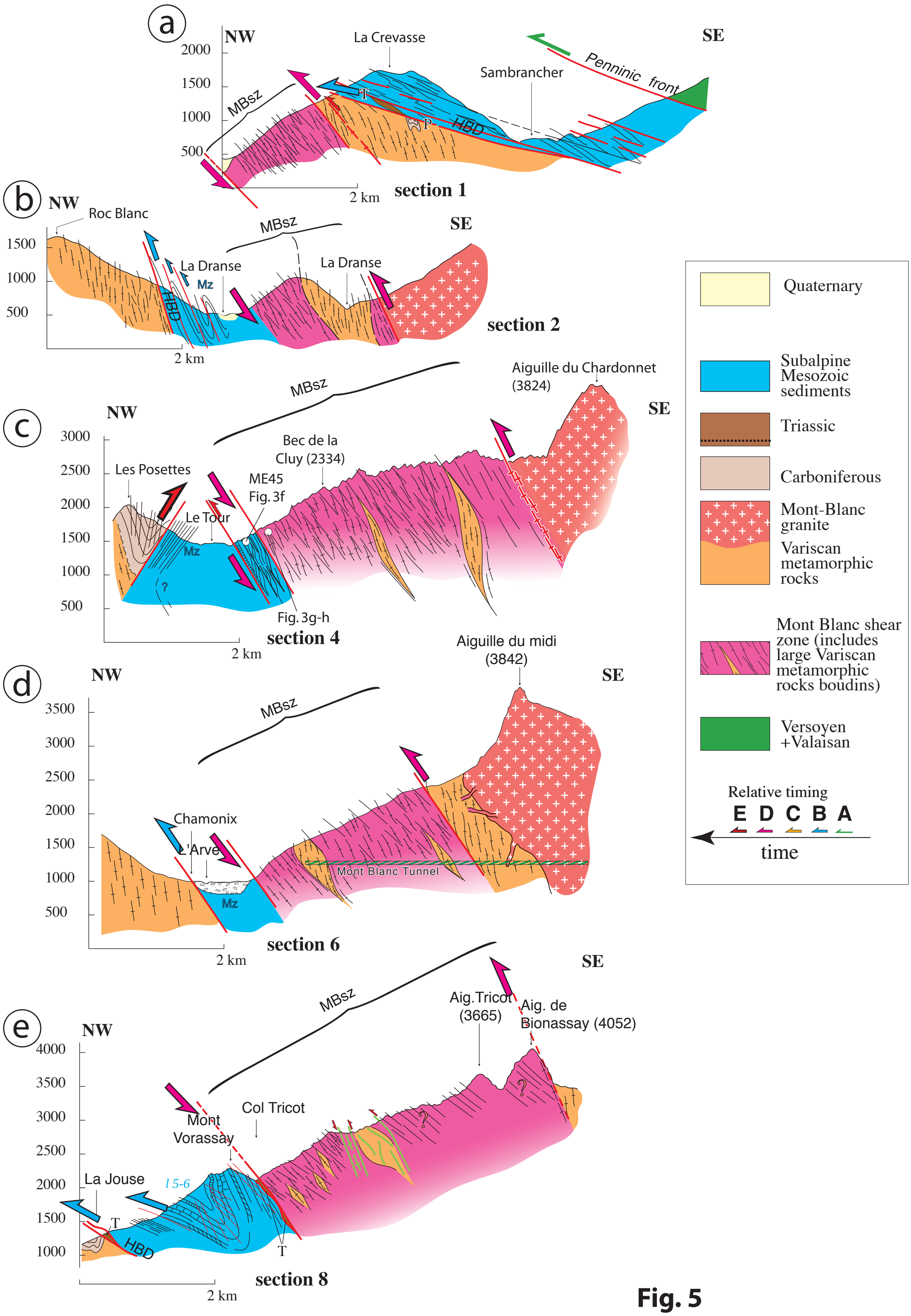

a
NW
SE
La Crevasse
Sambrancher
Penninic front
MBsz
HBD
section 1
2 km
b
Roc Blanc
La Dranse
Mz
MBsz
section 2
c
Aiguille du Chardonnet (3824)
Les Posettes
Le Tour
Bec de la Cluy (2334)
ME45 Fig. 3f
Fig. 3g-h
section 4
d
Aiguille du midi (3842)
Chamonix
L'Arve
Mont Blanc Tunnel
section 6
e
Aig. Tricot (3665)
Aig. de Bionassay (4052)
Mont Vorassay
Col Tricot
La Jouse
section 8
Quaternary
Subalpine Mesozoic sediments
Triassic
Carboniferous
Mont-Blanc granite
Variscan metamorphic rocks
Mont Blanc shear zone (includes large Variscan metamorphic rocks boudins)
Versoyen +Valaisan
Relative timing
E D C B A
time

Fig. 5

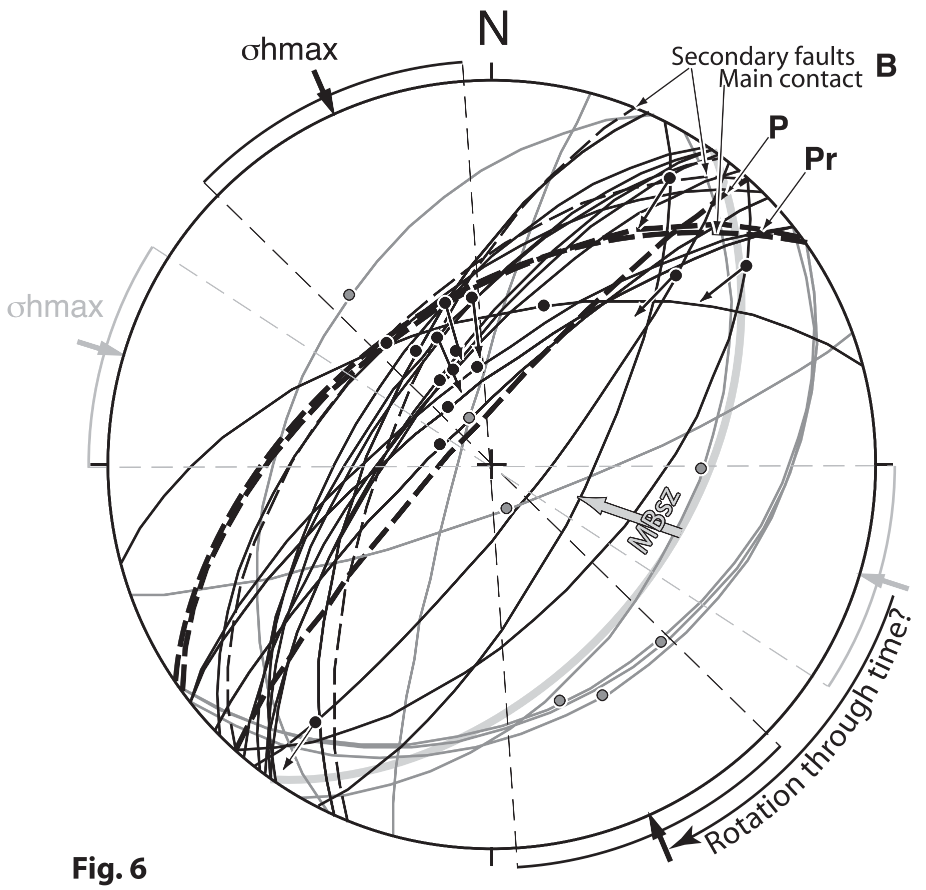
N
σhmax
σhmax
Secondary faults
B
Main contact
P
Pr
MBsz
Rotation through time?

Fig. 6

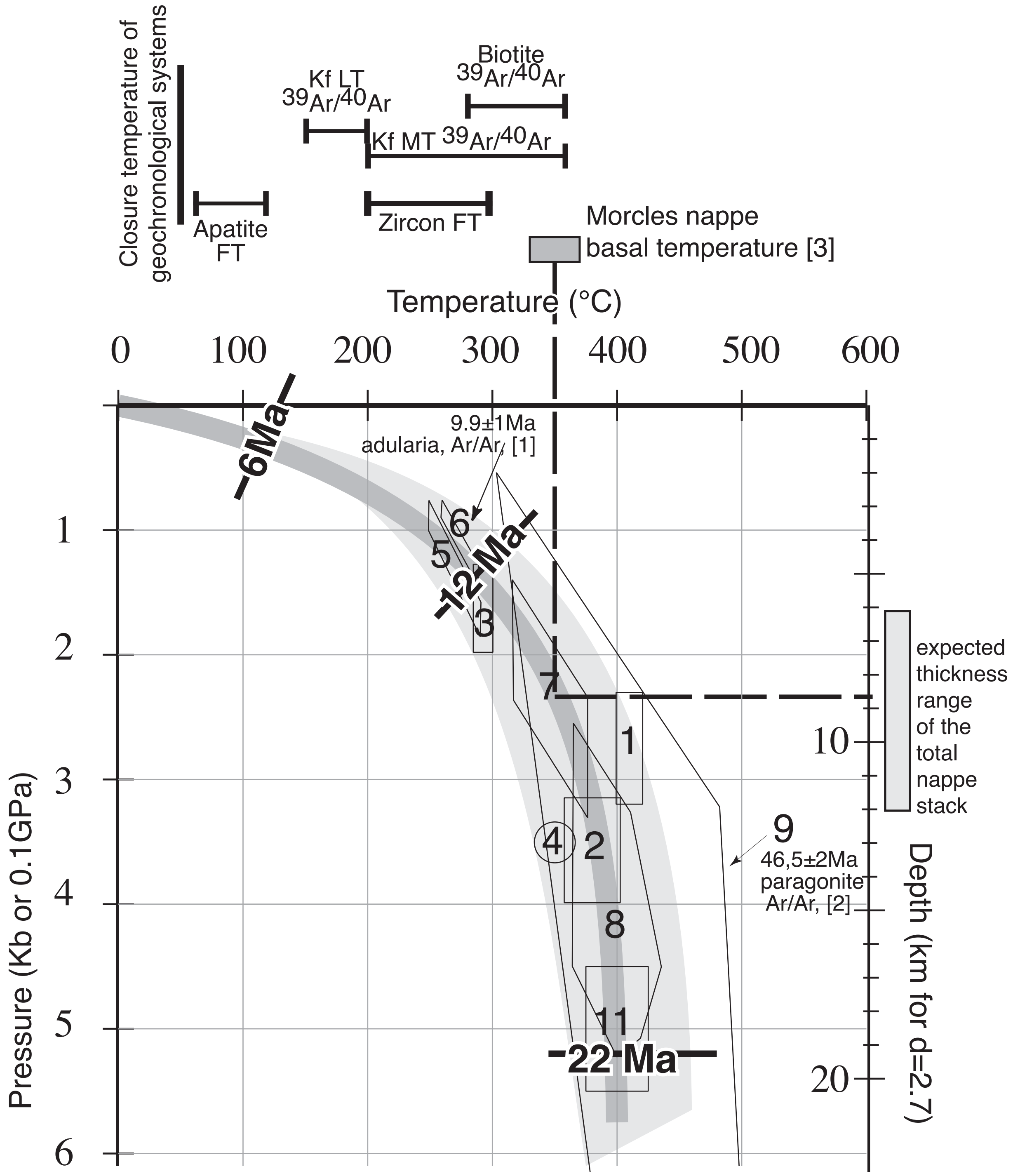
Closure temperature of geochronological systems
Apatite FT
Kf LT 39Ar/40Ar
Zircon FT
Kf MT 39Ar/40Ar
Biotite 39Ar/40Ar
Morcles nappe basal temperature [3]
Temperature (°C)
0 100 200 300 400 500 600
Pressure (Kb or 0.1GPa)
1 2 3 4 5 6
Depth (km for d=2.7)
10 20
-6Ma
-12 Ma
-22 Ma
9.9±1Ma adularia, Ar/Ar, [1]
46,5±2Ma paragonite Ar/Ar, [2]
expected thickness range of the total nappe stack
1 2 3 4 5 6 7 8 9 11

Fig. 7

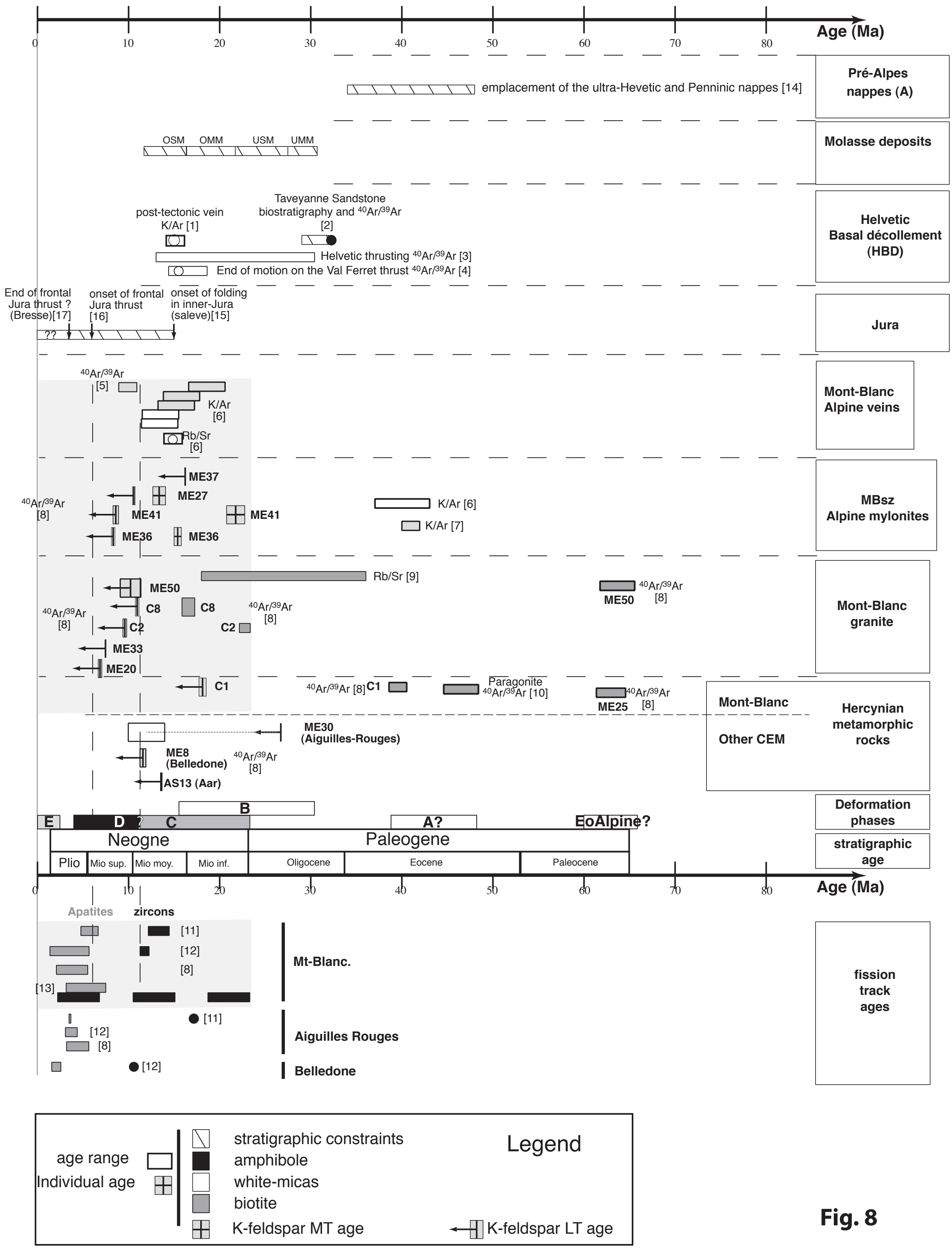

Age (Ma)
0
10
20
30
40
50
60
70
80
emplacement of the ultra-Hevetic and Penninic nappes [14]
Pré-Alpes nappes (A)
OSM
OMM
USM
UMM
Molasse deposits
post-tectonic vein K/Ar [1]
Taveyanne Sandstone biostratigraphy and $^{40}Ar/^{39}Ar$ [2]
Helvetic thrusting $^{40}Ar/^{39}Ar$ [3]
End of motion on the Val Ferret thrust $^{40}Ar/^{39}Ar$ [4]
Helvetic Basal décollement (HBD)
End of frontal Jura thrust ? (Bresse)[17]
onset of frontal Jura thrust [16]
onset of folding in inner-Jura (saleve)[15]
??
Jura
$^{40}Ar/^{39}Ar$ [5]
K/Ar [6]
Rb/Sr [6]
Mont-Blanc Alpine veins
ME37
ME27
$^{40}Ar/^{39}Ar$ [8]
ME41
ME41
ME36
ME36
K/Ar [6]
K/Ar [7]
MBsz Alpine mylonites
Rb/Sr [9]
ME50
C8
C8
$^{40}Ar/^{39}Ar$ [8]
C2
C2
$^{40}Ar/^{39}Ar$ [8]
ME33
ME20
ME50
$^{40}Ar/^{39}Ar$ [8]
Mont-Blanc granite
C1
$^{40}Ar/^{39}Ar$ [8] C1
Paragonite $^{40}Ar/^{39}Ar$ [10]
ME25
$^{40}Ar/^{39}Ar$ [8]
Mont-Blanc
Other CEM
Hercynian metamorphic rocks
ME30 (Aiguilles-Rouges)
ME8 (Belledone)
$^{40}Ar/^{39}Ar$ [8]
AS13 (Aar)
B
E
D
?
C
A?
EoAlpine?
Deformation phases
Neogne
Paleogene
Plio
Mio sup.
Mio moy.
Mio inf.
Oligocene
Eocene
Paleocene
stratigraphic age
Age (Ma)
Apatites
zircons
[11]
[12]
[8]
[13]
Mt-Blanc.
[11]
[12]
[8]
Aiguilles Rouges
[12]
Belledone
fission track ages
Legend
age range
Individual age
stratigraphic constraints
amphibole
white-micas
biotite
K-feldspar MT age
K-feldspar LT age

Fig. 8

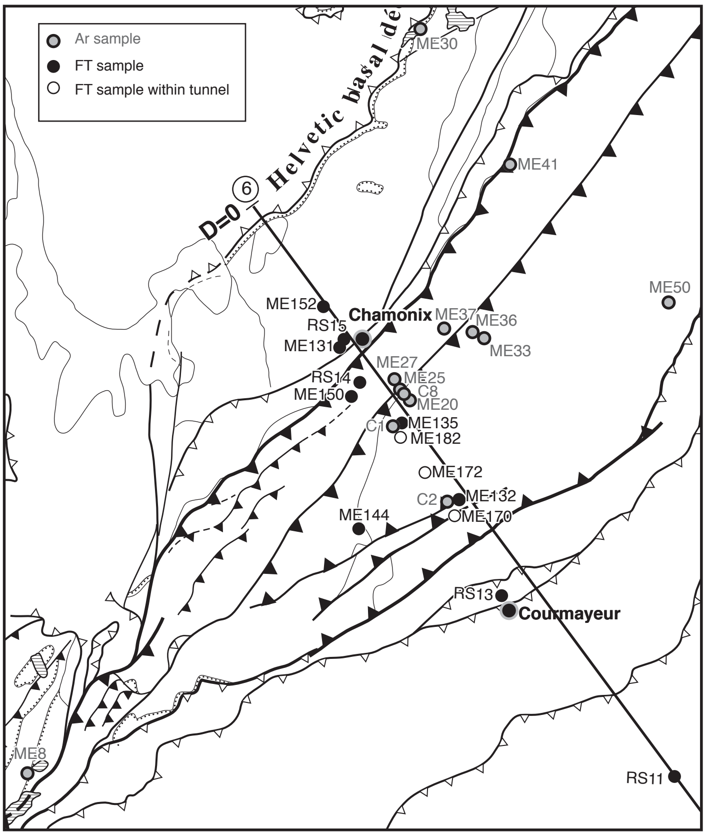

Ar sample
FT sample
FT sample within tunnel
D=0
6
Helvetic basal dé
ME30
ME41
ME50
ME152
Chamonix
RS15
ME131
ME37
ME36
ME33
ME27
RS14
ME150
ME25
C8
ME20
C1
ME135
ME182
ME172
C2
ME132
ME170
ME144
RS13
Courmayeur
ME8
RS11

Fig. 9

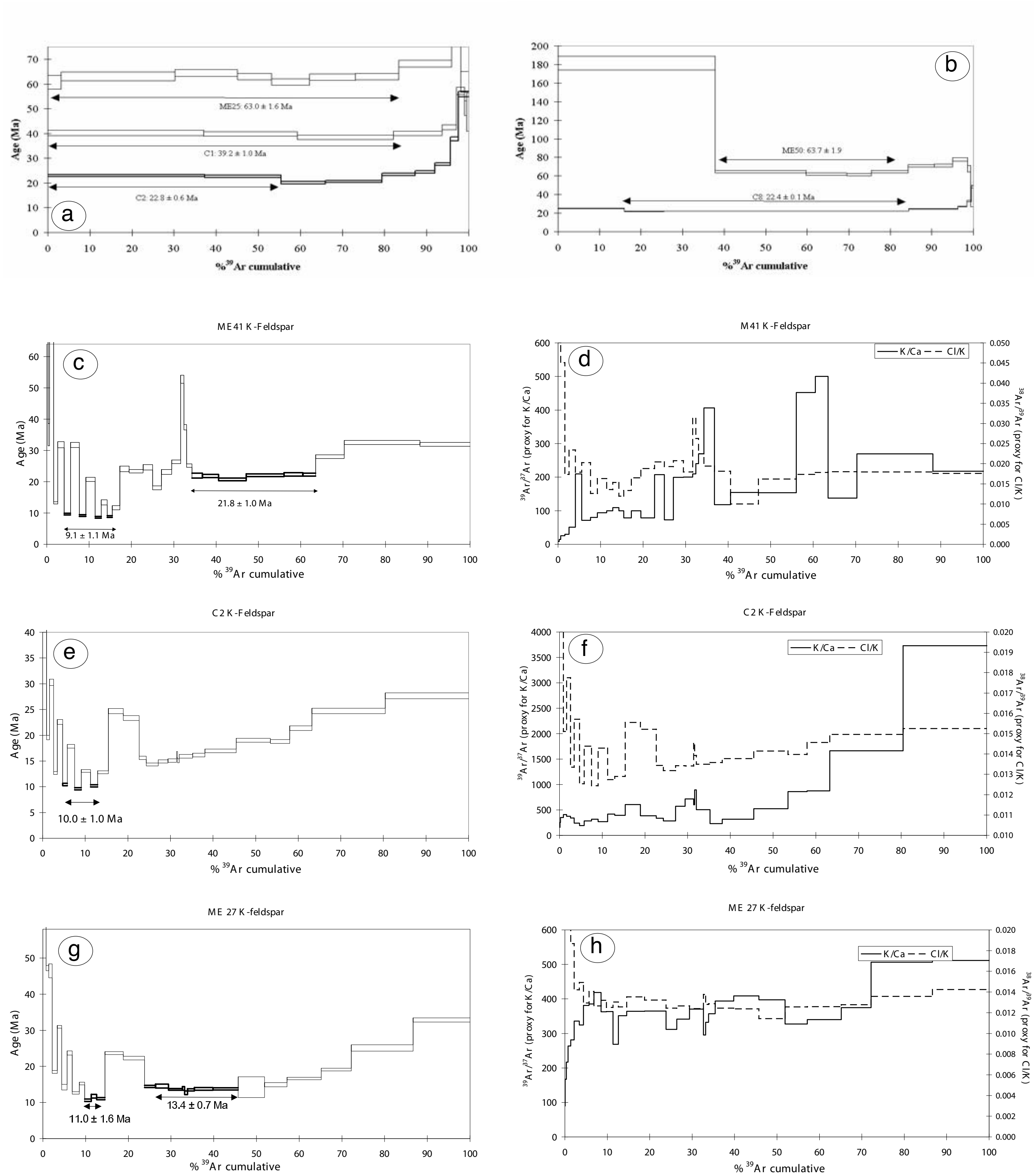
a
b
ME25: 63.0 ± 1.6 Ma
C1: 39.2 ± 1.0 Ma
C2: 22.8 ± 0.6 Ma
ME50: 63.7 ± 1.9
C8: 22.4 ± 0.1 Ma
Age (Ma)
%39Ar cumulative
ME41 K-Feldspar
c
21.8 ± 1.0 Ma
9.1 ± 1.1 Ma
M41 K-Feldspar
d
K/Ca
Cl/K
39Ar/37Ar (proxy for K/Ca)
38Ar/39Ar (proxy for Cl/K)
C2 K-Feldspar
e
10.0 ± 1.0 Ma
f
ME 27 K-feldspar
g
11.0 ± 1.6 Ma
13.4 ± 0.7 Ma
h

Fig. 10

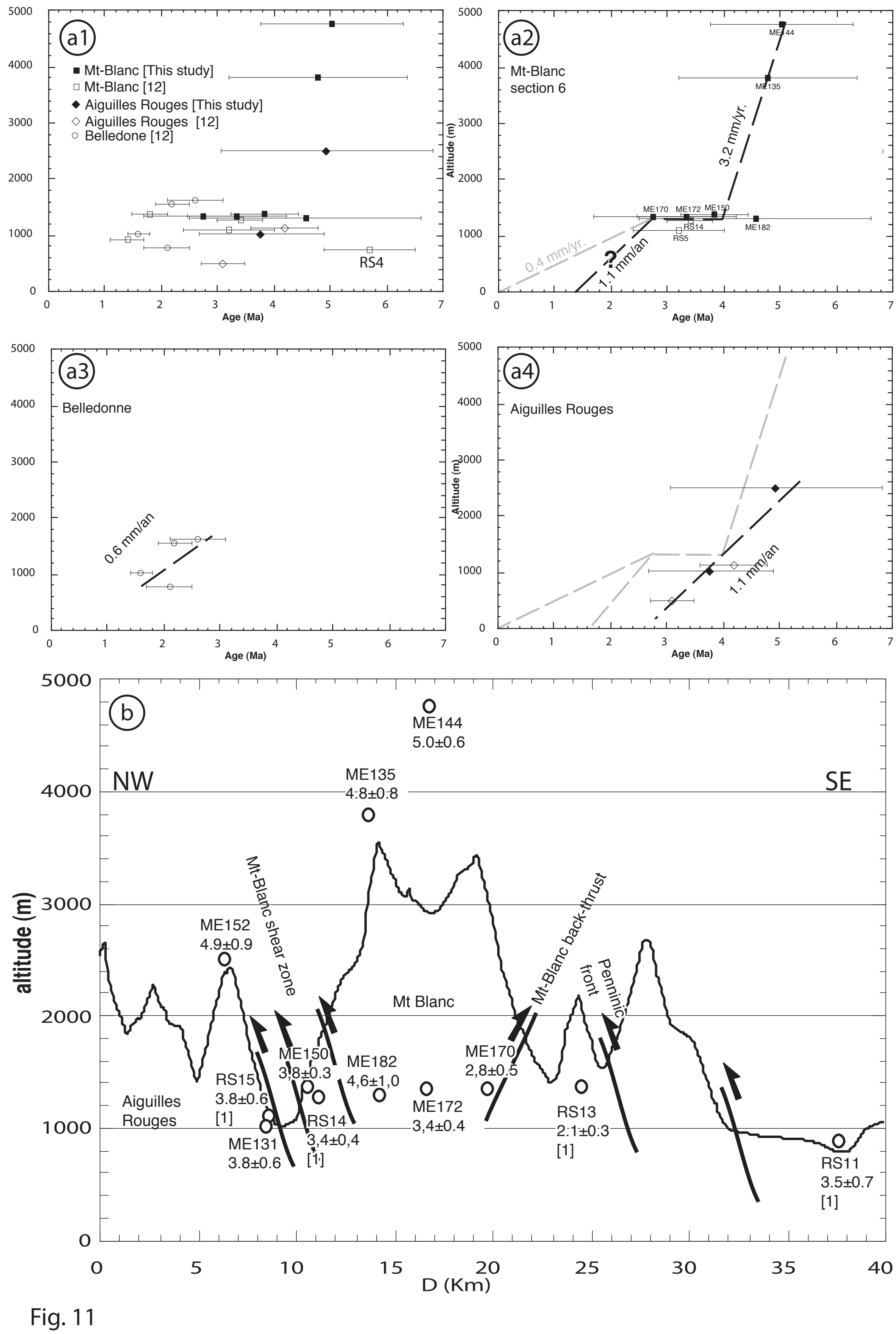

a1
Mt-Blanc [This study]
Mt-Blanc [12]
Aiguilles Rouges [This study]
Aiguilles Rouges [12]
Belledone [12]
RS4
a2
Mt-Blanc
section 6
3.2 mm/yr.
0.4 mm/yr.
1.1 mm/an
a3
Belledonne
0.6 mm/an
a4
Aiguilles Rouges
1.1 mm/an
Altitude (m)
Age (Ma)
b
NW
SE
ME144
5.0±0.6
ME135
4.8±0.8
ME152
4.9±0.9
Mt-Blanc shear zone
Mt Blanc
Mt-Blanc back-thrust
Penninic front
ME150
3,8±0.3
ME182
4,6±1,0
ME170
2,8±0.5
RS15
3.8±0.6
[1]
Aiguilles Rouges
ME131
3.8±0.6
RS14
3,4±0,4
[1]
ME172
3,4±0.4
RS13
2.1±0.3
[1]
RS11
3.5±0.7
[1]
altitude (m)
D (Km)

Fig. 11

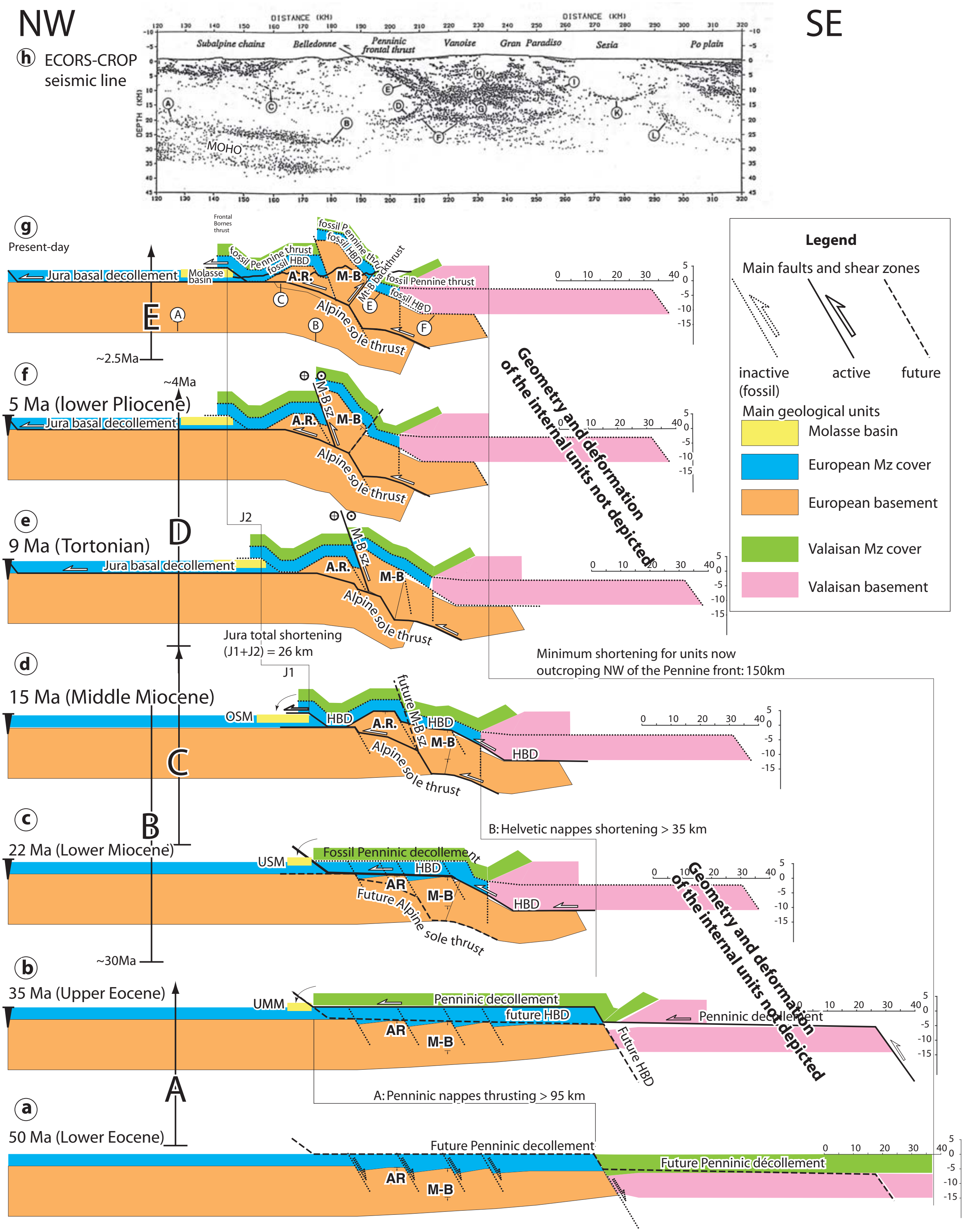

NW
SE
h ECORS-CROP seismic line
Subalpine chains
Belledonne
Penninic frontal thrust
Vanoise
Gran Paradiso
Sesia
Po plain
MOHO
g Present-day
Jura basal decollement
Molasse basin
fossil Pennine thrust
fossil HBD
A.R.
M-B
M-B backthrust
Alpine sole thrust
E
~2.5Ma
f 5 Ma (lower Pliocene)
~4Ma
M-B sz
e 9 Ma (Tortonian)
D
J2
Jura total shortening (J1+J2) = 26 km
d 15 Ma (Middle Miocene)
J1
OSM
HBD
future M-B sz
C
B: Helvetic nappes shortening > 35 km
c 22 Ma (Lower Miocene)
B
USM
Fossil Penninic decollement
AR
Future Alpine sole thrust
~30Ma
b 35 Ma (Upper Eocene)
UMM
Penninic decollement
future HBD
Future HBD
A
A: Penninic nappes thrusting > 95 km
a 50 Ma (Lower Eocene)
Future Penninic decollement
Future Penninic décollement
Geometry and deformation of the internal units not depicted
Minimum shortening for units now outcroping NW of the Pennine front: 150km
Legend
Main faults and shear zones
inactive (fossil)
active
future
Main geological units
Molasse basin
European Mz cover
European basement
Valaisan Mz cover
Valaisan basement

Fig.12